

R. D. Barree

By

DEVELOPMENT OF A NUMERICAL SIMULATOR FOR
THREE-DIMENSIONAL HYDRAULIC
FRACTURE PROPAGATION IN HETEROGENEOUS MEDIA

A dissertation submitted to the Faculty and the Board of Trustees of the Colorado School of Mines in partial fulfillment of the requirements for the degree of Doctor of Philosophy (Petroleum Engineering).

Golden, Colorado
Date April 10, 1984

Signed: Robert D. Barree

Approved: Dr. J. W. Gratton
Thesis Advisor

Golden, Colorado
Date April 10, 1984

George W. Van Kirk
Dr. C. W. Van Kirk
Head of Department of
Petroleum Engineering

Factors affecting fracture geometry and propagation include Young's Modulus, Poisson's Ratio, and tensile strength of the rock, principal confining stresses in the earth, pore pressure, fracture fluid viscosity, fluid leakoff, and injection rate. Fluid flow in the fracture is calculated using a two dimensional finite difference formulation. Rock properties and stresses are assigned at each node of the finite difference grid. Deformation of the fracture face at each grid point is calculated using an integral equation which assumes a distributed load over the face of a semi-infinite elastic solid. A zero displacement condition is applied at the boundary of the fracture. The pressure and width calculations are coupled sequentially. An implicit pressure solution is followed by an explicit evaluation

A numerical simulator for the propagation of hydraulically induced fractures is presented. The simulator is capable of predicting three-dimensional fracture geometry, during propagation, as a function of time. The medium through which the fracture propagates is assumed to be linearly elastic. Random heterogeneity can be included in a modified system.

ABSTRACT

Along with the fracture propagation model, a stand-alone program capable of calculating the fracture width distribution resulting from a pre-selected pressure distribution is presented. This system allows easy determination of the sensitivity of fracture width to various parameters.

of the pressure solution is obtained. The system is solved iteratively until convergence of the integral equation for fracture width at each grid point.

ABSTRACT iii

LIST OF FIGURES. viii

LIST OF TABLES xi

ACKNOWLEDGEMENTS xii

INTRODUCTION 1

REVIEW OF PERTINENT LITERATURE 3

Theories of Elasticity and Rupture. 3

Review of Existing Fracture Models. 8

NEW FORMULATION BASED ON CLASSICAL ELASTIC THEORIES 23

Details of Mathematical Formulation 26

RESULTS OF STATIC MODEL CALCULATIONS 36

Comparison of Fracture Width Prediction With Sneddon's Equation 36

Comparison of Current Model With Previous Models for Various Fracture Length/Height Ratios 41

Effects of Variations of Elastic Properties and Confining Stresses on Calculated Fracture Widths 49

Effects of Grid Size on Fracture Geometry 56

Page

TABLE OF CONTENTS

NUMERICAL CHARACTERISTICS OF DYNAMIC PROPAGATION

MODEL 62

Discussion of the Numerical Stability of the

Dynamic Model. 62

Time Requirements of the Numerical Model. 66

DYNAMIC FRACTURE PROPAGATION STUDIES 68

Fracture Growth from Various Points of

Initiation 68

Hypothetical Studies of Fracture Containment 71

Effects of Confining Stress. 72

Effects of Elastic Properties. 75

Effects of Tensile Strength. 78

COMPARISON OF DYNAMIC GROWTH MODEL WITH EXPERIMENTAL

RESULTS 82

Effects of Fracturing Fluid Properties. 88

Viscosity Effects. 88

Density Effects 90

CONCLUSIONS. 92

RECOMMENDATIONS FOR FUTURE RESEARCH. 94

NOMENCLATURE 96

REFERENCES 99

APPENDICES

A. DERIVATION OF THE FRACTURE WIDTH EQUATION. . . 104

B. DERIVATION OF THE PRESSURE EQUATION
FOR FLUID FLOWING IN THE FRACTURE. . . 113

LIST OF FIGURES

Page

1. Grid Used to Model a Radially Symmetrical Pressurized Fracture 37

2. Normalized Fracture Width Versus Radius for a Symmetric, Constant Pressure, Circular Fracture. 39

3. Schematic of Model Fracture Showing Principal Dimensions for Comparison with Classical Width Equations. 43

4. Fracture Widths Obtained from PKN, GGD, and Current Models for Various Fracture Aspect Ratios 45

5. Normalized Width versus Normalized Length Profiles for Various Length/Height Ratios 48

6. Assumed Geometry for Confining Stress Variation Study, After Hansen, et al (40). 50

7. Normalized Fracture Width versus Normalized Length for Various Depths of Penetration Into a High Confining Stress Layer. 52

8. Effect on Fracture Width of Partial Penetration Into a Layer of Higher Young's Modulus 53

9. Effect of Variation in Poisson's Ratio on Calculated Fracture Widths. 55

10. Effect of Node Size on Calculated Fracture Geometry 57

11. Effect of Ratio of Boundary Area to Fracture Area on Calculated Fracture Widths 59

85 Top-Stressed Ash-Fall Tuff Samples

19. Comparison of Predicted and Experimental Frac-
 ture Propagation in a) Bottom-Stressed and b)
 Lower Half, and b) Stress Applied to Upper
 Half 84

18. Representation of Stress Distribution in Ash-
 Fall Tuff Samples with a) Stress Applied to
 Lower Half, and b) Stress Applied to Upper
 Half 80

17. Effect of Tensile Strength Variation on Frac-
 ture Containment in a Layered System 80

16. Effects of Elastic Property Variation on
 Fracture Containment 77

15. Effect of Difference in Confining Stress in
 Adjacent Layers on Fracture Containment. 73

14. Effect of Point of Initiation on Early Time
 Fracture Growth. 70

13. Demonstration of Convergence of Current Model by
 Comparison with PKN Solution 65

12. Increase in Boundary Node Stress for Various Rela-
 tive Magnitudes of Fracture Boundary and Pres-
 surized Fracture 60

20. Simulation Results of Fracture Propagation in Layered Tennessee Sandstone Samples Under a) No Confining Stress, b) 250 psi Stress on Lower Section, and c) 1000 psi Stress on Upper Section. 87

A1. Solution of General Integral Equation for Fracture Geometry. 107

A2. Evaluation of Double Integral Geometrical Factor as a Function of Distance From the Point of Interest. 110

B1. Description of an Individual Grid Node 114

B2. Five Point Finite Difference Grid Showing Sign Convention for Inflow 116

1. Fracture Widths Obtained by GFD and PKN Width	
Equations Normalized to Current Model Pre-	
dictions for Various Length-Height Ratios. . . .	47
	<u>Page</u>

LIST OF TABLES

I would like to acknowledge Marathon Oil Company for its generous support throughout my pursuit of this degree and to express appreciation for the use of its computing facilities in the development of the numerical models presented here. I would also like to thank Dr. R. W. Wiley for his suggestions and discussions on this topic. Many thanks are also due to Kathy England for her help and dedication in typing this manuscript. Finally, I would like to express my appreciation for the continuous understanding and support of my wife, Valencia, throughout the duration of this work.

ACKNOWLEDGEMENTS

Hydraulically-induced fractures have been used for nearly forty years to increase productivity of producing wells, especially in low permeability formations, or to increase injectivity in water injection wells. Recently hydraulic fracturing technology has been applied to increase both productivity and recoverable reserves in low permeability gas reservoirs. Estimates claim hydraulic fracturing can produce additional reserves in these low permeability formations roughly equal to current reserve estimates for conventional gas reservoirs (1). With the increased use and expense of hydraulic fracturing as a well stimulation technique, it is desirable to have the ability to design an efficient fracturing treatment in a complex lithologic system.

Most models currently used in the design of hydraulic fracture treatments rely on simplifying assumptions, particularly that of constant, known fracture height. The hydraulically fractured formation is generally assumed to be homogeneous and linearly elastic. Work presented in this dissertation is directed toward relaxing or eliminating some of the simplifying assumptions which are commonly made. The goal is to produce a more general three dimensional model of fracture propagation in heterogeneous systems.

INTRODUCTION

Models which are currently applied to the design of hydraulic fracture geometries are described. These models are, in some cases, used as a basis for development of the current work, or as examples of the types of simplifications which have been made in the past. Derivations of a general formulation for predicting three dimensional fracture geometry during propagation is presented. This formulation is based on classical linear-elastic theories.

Results of model studies using the current formulation are presented to show the effects of variations in rock and fluid properties on fracture propagation, geometry, and confinement. Experimental data published by other researchers are used to verify the applicability of the model.

The work of A. A. Griffith is commonly cited as the basis for modern theories of rupture in elastic solids. The fundamental concept underlying his theory of rupture is that solids, like liquids, exhibit some surface or interfacial tension (2,3,4). Given that the surface tension of any substance is zero at the critical temperature and pressure, Griffith hypothesized that the strain energy required to rupture a solid must be equal to the amount of work done against cohesive forces in raising the substance to its critical temperature and pressure. In general, this energy requirement is of the same order as the total heat of vaporization of the material (3). Griffith attributes the difference in the observed and theoretical amounts of energy required to cause rupture in elastic solids to the existence

Theories of Elasticity and Rupture:

The literature on the subject of rock mechanics and fracture spans a long period of time. The publications reviewed here appear in roughly chronological order. Special notice should be given to the works of Sneddon (4,6) in the field of rock mechanics, and Perkins and Kern (13), Geertsma and de Klerk (15), and Nordgren (16) in the field of hydraulic fracture modeling. These authors have provided the most significant contributions to current expertise.

REVIEW OF PERTINENT LITERATURE

of a large number of micro-cracks or flaws in every material. Combining this theory with an energy balance relating change in strain energy to change in potential energy caused by creating new fracture surface, Griffith presents a criterion for rupture of a flawed elastic medium. Conditions of rupture are calculated by Griffith for a mathematical crack in an infinite elastic solid. For his purposes, the crack is modeled as an ellipse of zero eccentricity (i.e., the ratio of the minor and major axes of the ellipse is zero) under conditions of "plane strain". The plane strain condition requires that displacements normal to the plane of the ellipse are zero.

The condition of rupture developed by Griffith was extended to three dimensions by Sack assuming radial symmetry (5). The problem was later approached by Sneddon who also modeled the crack as a flat ellipsoid of revolution (4, 6). In addition to calculating the stresses in the vicinity of a pressurized crack, he also derived expressions for the displacements of the crack surfaces under conditions of constant internal pressure and pressure varying radially from the center of the crack. The solution assumes that the pressure is applied over a circular area of radius R , on the plane, $z = 0$, of a semi-infinite half space ($z \geq 0$). The surface of the half space is subjected to the following conditions:

This equation is of great importance in the development of many fracture models, as will be shown later. Normal displacement of the surfaces of a plane strain linear crack were studied by England and Green (7). They approached the problem from both the viewpoint of a linear crack in an unbounded medium and a row of punches on the

u = displacement of loaded surface
 v = Poisson's Ratio
 E = Young's Modulus
 P_0 = pressure applied to plane
 R = radius of pressurized circle
 y = coordinate in the plane.

where

$$u = \left[\frac{E}{2(1-\nu^2)P_0} \sqrt{R^2 - y^2} \right] \quad [1]$$

ment of the plane under constant pressure is:

The equation derived by Sneddon (6) for normal displace-

ment of the plane.

where τ_{xy} is shear stress in the x-y plane, σ is the normal stress applied to the x-y plane, and u is the displacement of the plane.

$$\begin{aligned} (1) \quad \tau_{xy} &= 0; & \text{for all } y \\ (II) \quad \sigma &= -p(y); & y < R \\ (III) \quad u &= 0; & y \geq R \end{aligned}$$

pressure loss per unit length is proportional to the cube of
tion. Assuming Poisseulle flow between parallel plates, the
flowing pressure distribution inside a crack during propaga-
This concept is physically justified by considering the
crack which is unpressured.

there is a small area near the tip or leading edge of the
According to Barenblatt, a smooth closure can only occur if
close smoothly to avoid this infinite stress concentration.
cannot conform to the classical elliptical shape, but must
Barenblatt states that the tips of a real equilibrium crack
the tensile stress at the boundary of the crack is infinite.
pressure inside the elliptical crack, calculations show that
ready defined by Sneddon and others. Assuming a constant
stress field in the vicinity of an elliptical crack, as al-
by Griffith. His finding is based on the analysis of the
an equilibrium crack cannot exist given the geometry assumed
Barenblatt (8). A primary conclusion of this work is that
elastic solids is concisely documented in a paper by G. I.
A large body of Russian work in the area of rupture of
equation under conditions of constant pressure.

discussed later, the equation simplifies to the Sneddon
is commonly used in fracture model development. As will be
for displacement in a crack opened by non-constant pressure
surface of a semi-infinite space. Their resultant equation

the separation between the plates (9). Thus, there is a small area near the fracture tip in which a large pressure drop occurs. This corresponds to the essentially unpressurized area in which the smooth closure of the fracture faces occurs. According to Barenblatt, this smooth closure of the ends of a fracture can only be accomplished with a finite stress concentration by the existence of the unpressurized tip. A direct result of the conclusion reached by Barenblatt is that, in the absence of other factors such as fluid leakage, or high tensile strength of the fractured medium, an equilibrium crack can only exist in a dynamic condition, i.e., when there is a flowing pressure gradient in the fracture. If injection into the fracture is stopped, the fluid contained in the fracture will advance into the unpressurized tip thus increasing the tensile stress at the fracture boundary and extending the fracture. This mechanism would lead to continued expansion of the fracture area until the width completely collapses. In an impermeable medium this would appear to generate a fracture length approaching infinity. This conclusion is not well addressed by the authors of the hypothesis (10). Fracture growth in this situation could be plausibly limited by a finite tensile strength of the medium.

Barenblatt's theory for stability of hydraulic fractures, i.e., partial pressurization by the fracture fluid, is derived from ideas used in one of the earliest fracture models. This model, proposed by Khristianovich and Zheltov, assumes a constant pressure over part of the fracture length (11). The constant pressure is calculated so that the total load on the fracture walls is statically equivalent to that generated by the continuous, flowing fluid pressure. A statically equivalent load is one whose resultant is equal to the resultant of the continuous pressure distribution and is applied at the same point. The fracture geometry is calculated using the assumed pressure distribution subject to the conditions of finite stress at the fracture tip. A conformal mapping technique proposed by J. Muskhelishvili is used in the geometry calculations. The fracture is assumed to have a roughly elliptical cross-section in horizontal planes and a rectangular section in vertical planes. Fracture propagation rate is related to injection rate through a material balance equation.

A simple fracture model, which is interesting from the standpoint of the current work, is presented by Yu. N. Vasil'ev (12). The model proposes that in a jointed carbonate formation, a vertical fracture face can be modeled as a

equation developed by Sneddon for a radially symmetric similar development (13). These authors applied the width made by Perkins and Kern based on what must be considered a model developments. However, an important contribution was half space, it's almost nowhere referenced in later fracture application of the equations for deformation of an infinite Although Vasil'ev's model represents an interesting

will vary with the fourth root of flow rate. The conclusion of the paper is that maximum fracture width faces are used to relate fracture width to injection rate. for fluid in laminar flow between the converging fracture the points of application of the forces. Pressure losses linear locus of zero displacement bisecting the line between placements caused by the two opposed forces results in a from the original load, so that superposition of the distance assumes an equal and opposite normal load at some distance fracture is accounted for by superposition. Vasil'ev The effect of the zero displacement boundary of the

assumptions involved are similar to those used by Sneddon. nite half space acted on by a normal load. The equation and is derived from the displacement of the surface of an infi- determined by J. Boussinesq, in about 1885. This equation width of the fracture can be calculated using an equation rectangle with a known height and some presumed length. The

When the fracture reaches confining layers, presumably zones of higher stress, the fracture will propagate upwards and downwards into these zones until an equilibrium condition is reached. The equilibrium state is likened to that support this conclusion.

Data are presented by these authors which fracture extension pressure should vary as the fifth root of Sneddon's equation for fracture volume to conclude that phase, they apply Sack's fracture extension criterion and growth will be confined. During this radial expansion it reaches some region of higher stress where its vertical cal fracture initiated at a point will expand radially until analysis of fracture propagation. They reason that a vertical fracture boundary (6).

The work of Perkins and Kern is primarily a combination of the deformation equation of Sneddon (6), the rupture criteria proposed by Griffith (3) and Sack (5), and a practical analysis of fracture propagation. They reason that a vertical fracture boundary (6).

It is worth reiterating that this equation was developed from the same equations used by Vasil'ev. One major difference involves the assumption of radial symmetry, rather than a rectangular geometry. The other difference is that Sneddon relies on an infinite tensile stress distribution along the boundary of the fracture rather than a finite tensile stress centered at a point at some distance from the fracture boundary (6).

tip of the crack is thus spread over a plastically deformed nated. According to their theory, the tensile stress at the elastic manner so that the infinite tensile stress is limited that an area surrounding the crack tip must behave in an insulating from the use of Sneddon's equation. They conclude condition of infinite stress at the boundary of a crack re-

In a later paper Perkins and Knech (14) address the calculations of fracture length are given.

ting fracture width as a function of injection rate. No width equations, the authors propose a method for calculating regimes are also derived. By coupling the fluid flow and fracture. Expressions for pressure loss under various flow width is completely controlled by the fluid pressure in the be constant and known. By this assumption the fracture will be confined and that when this occurs the height will Further development of the model assumes that the fracture that of a radially symmetric fracture of the same height. that the width of a vertically confined fracture is equal to Using Sneddon's width equation, Perkins and Kern assume

then propagate laterally through the zone of lower stress. they can stop the vertical growth of the fracture which will stress at the tip. If the confining layers are thick enough against the fracture wall is balanced by the high confining of a lever at static equilibrium in that the fluid pressure

model is not widely applicable. cause of the expected rarity of horizontal fractures, this fractures using Sneddon's equation is also described. Be- section (11). A model for radially propagating horizontal Zheltov, i.e., constant fracture width over any vertical geometry superficially like that used by Khrisitianovich and Geertsma and de Klerk (15). They assume a vertical fracture the standpoint of its general acceptance, is presented by One of the most important fracture design models, from

ples are given to illustrate the utility of the model. al data from breakdown of radial cracks in laboratory sam- change in fracture (or injected fluid) volume. Experiment- equation relating change in surface area of the fracture to placement calculations are coupled with an energy balance results in zero displacement at the crack tip. The dis- stress and inelastic yielding in the stress altered region Sneddon in the assumption that the distributed tensile infinite solid. The calculations differ slightly from assuming a radially symmetric load on the surface of a semi- Displacement of the crack surfaces are again calculated

the tensile strength of the rock. veloped where all tensile stresses are finite and limited by ories, they show that a stable equilibrium crack can be de- tional to the applied stress on the crack. Using these the- region. The width of the stress altered region is propor-

The width of a vertical fracture is determined as a function of pressure distribution and length by the plane strain solution developed by England and Green (7). This equation yields a fracture shape which is elliptical in horizontal planes. The boundary condition, or rupture criterion, of Khristianovich and Zheltov, which was extended by Barenblatt, is applied to the fracture width equation (11, 8). An important result of the use of this equation for the assumed geometry is that the fracture width increases in proportion to the fracture length. Additionally, width is independent of fracture height.

Fluid pressure drop along the fracture is calculated assuming linear flow between parallel plates. Fracture length, width and internal pressure are related by material balance. It is interesting to note that the width equation used by Geertsma and de Klerk reduces to the Sneddon equation under the assumption of constant pressure:

$$w = \frac{G}{2(1-\nu) L \Delta P} \quad [2]$$

where

w = fracture width at wellbore

L = fracture length

$$G = E/2(1+\nu)$$

substituting for G in the equation yields:

Comparison of this with the width equation of Geertsma and de Klerk shows a difference of a factor of two. This dif-

$$w = \frac{E}{2(1-\nu^2)H\Delta P} \quad [5]$$

After substituting for G the equation is:

$$w = \frac{G}{(1-\nu)H\Delta P} \quad [4]$$

by Perkins and Kern, for fracture width at the wellbore is: equation cited by Nordgren, which is identical to that given radial symmetry of the fracture had to be assumed (13). The work, it is apparent that in using Sneddon's derivation, planes is used. Recalling the discussion of the earlier he states that an assumption of plane strain in vertical equation presented by Perkins and Kern is used by Nordgren, estimation of fracture length (16). Although the width on an extension of the work of Perkins and Kern to allow the A fracture model presented by R. P. Nordgren is based fracture.

infinite half space rather than the width of a two-sided Sneddon's calculation of the displacement of one face of an factor of two. This apparent difference results from Comparison with Sneddon's equation shows a difference of a

$$w = \frac{E}{4(1-\nu^2)L\Delta P} \quad [3]$$

the discussion by T. K. Perkins and the authors' reply. A
One of the most interesting features of the paper is

obtained by Daneshy's model are presented by Daneshy (18).
Nordgren's and Geertsma and de Klerk's methods with those
fracture geometries calculated using Perkins and Kern's,
calculating statically equivalent loads. Comparisons of
by Khristianovich and Zheltov (11) with other methods of
voted to comparisons of various pressure functions proposed
of more rigorous numerical methods (18). Much effort is de-
the model of Geertsma and de Klerk through the application
A. A. Daneshy presents a fracture model which extends

of time.

length and width at the wellbore are calculated as functions
sure distribution along the fracture from which fracture
tion rate, the fluid flow and leakoff equation give a pres-
(17). Using an assumed constant fracture height and injec-
walls is also included using the method of Howard and Fast
elliptic cross section. Fluid loss through the fracture
drop equation assuming Newtonian, laminar flow through an
Nordgren couples the width equation with the pressure
height $(H/2)$ is used in Nordgren's equation.

the radius of the loaded circle, thus the fracture half-
tion. Sneddon's radial symmetry assumption relates width to
ference arises from the use of the length term in the equa-

point made in the authors' reply, which has been made repeatedly here, is that almost all fracture models presented to date rely on the equations developed by Sneddon or England and Green. Daneshy identified the width equation used by Khristianovich and Zheltov as that proposed by England and Green (18).

In the author's reply to Perkins' discussion, Daneshy gives the Sneddon width equation as:

$$w = \left[\frac{E}{4(1-\nu^2)} \right] \Delta p H \quad [6]$$

and the England and Green equation as:

$$w = \left[\frac{E}{4(1-\nu^2)} \right] \Delta p L \quad [7]$$

This form of Sneddon's equation differs from that previously given, and is in error. As noted here and by Geertsma and Haakens (19), in their excellent comparative paper, the value of H in Eq. 6 should be replaced by $H/2$ to conform to the radial symmetry assumption made by Sneddon. Geertsma and Haakens derive equations for widths and lengths of vertical fractures as predicted by these two methods. For a single wing fracture they are:

$$L = 15.858 \left[\frac{G \rho_3}{G \rho_4} \right]^{1/5} H^{4/5} \quad [8]$$

[9]

$$w = 0.1072 \left[\frac{G_H}{(1-\nu) Q^2} \right]^{1/5} t^{4/5}$$

for Nordgren's model and:

[10]

$$L = 9.382 \left[\frac{G Q^3}{n (1-\nu) H^3} \right]^{1/6} t^{2/3}$$

[11]

$$w = 0.1355 \left[\frac{G_H^3}{(1-\nu) n Q^3} \right]^{1/6} t^{1/3}$$

for the Geertsma and de Klerk model.

In a general comparison of the results obtained from

the major types of fracture models, Daneshy states that the

Perkins-Kern-Nordgren (PKN) models predict a treating pres-

sure which must increase with time. Conversely, the

Geertsma-deKlerk type model predicts a treating pressure

which decreases with pumping time. Daneshy finds the latter

behavior more consistent with his personal observations

(18). Geertsma and Haafkens (19) have quantified these ob-

servations. They derive equations showing that the Nordgren

type model predicts a wellbore pressure which varies with

fracture length as:

[12]

$$P_w = \sigma + \frac{H}{0.0585} \left[\frac{G Q^3}{n L} (1-\nu)^3 \right]^{1/4}$$

while Geertsma and de Klerk's model results in:

Many authors have applied the fracture geometry calculation used in the two general types of models discussed here. A. Settari presents a model which simultaneously calculates fracture propagation and geometry and two phase, two-dimensional fluid flow and heat transfer in a reservoir (20). This model, while theoretically applicable to any fracture geometry, assumes the Geertsma-de Klerk-Daneshy (GDD) fracture shape. Settari uses a sequential solution scheme to solve the various aspects of the reservoir-fracture interaction problem. This approach was extended somewhat by Nghiem, et al (21). They present the derivation for a fully implicit reservoir-fracture interaction model which also presupposes the GDD type geometry.

The PKN type geometry was extended by Advani using a finite element modeling technique (22). The fluid flow equations presented by Nordgren and the fracture geometry equations derived by Geertsma and Haekens for the PKN model were used to calculate transient fracture propagation by the finite element technique. The results were extended to the case of multi-layered formations using "scaling curves". These curves allow estimation of fracture width as a function

$$P^w = \sigma + \frac{H}{0.0221} \left[\frac{G \rho^u H}{3} \right]^{1/4} (1-\nu)^{3/2} \quad [13]$$

Factor. Fracture mechanics is taken into account in what
 ered systems is also determined using a stress intensity
 Geertsma and de Klerk. Equilibrium fracture height in lay-
 various width equations of the type used by Nordgren and
 terial balance equations developed by Nordgren coupled with
 et al (23-25). These authors utilize the fluid flow and ma-
 A similar modeling approach has been taken by Cleary,
 fracture geometry is not well defined by Advant.

material. The relation of this theoretical value to the
 in which T_0 is the surface tension of the fractured

$$K^2 = \frac{\pi E T_0}{(1-\nu^2)} \quad [14]$$

the stress intensity factor should be limited by K/π where:
 cohesion acting at the crack tip. Barenblatt theorizes that
 ment this term is related to the intensity of the forces of
 the stress intensity factor (8); According to his develop-
 stresses. Barenblatt discusses the theoretical nature of
 are related to fracture fluid pressure and in-situ earth
 tors at the fracture tips. These stress intensity factors
 height is obtained by calculating the stress intensity fac-
 ratio of elastic moduli are known. Equilibrium fracture
 dary layers where the difference in confining stress and
 tion of the depth of penetration of the fracture into boun-

Clearly calls a "leading edge model" (23). To simplify com-
 putation, the assumption of "self-similarity" is also made
 to allow spatial averaging of fracture geometry and to sim-
 plify evaluation of the storage term. An analytical or
 numerical relation of fracture height to time or position is
 also required by the model. This is usually obtained by
 separate solution of a vertical cross-sectional model.
 Height growth information generated by this model can then
 be included in the larger model. Design equations have been
 sufficiently simplified by these approximations that a
 "pseudo three-dimensional" fracture design model has been
 written for a hand-held microcomputer (24). The method has
 been extended to a "fully three-dimensional" model which is
 applicable to vertically confined fractures (25).

Other authors have attempted the calculation of frac-
 ture geometry assuming two-dimensional plane strain charac-
 teristics (26-28). Hanson, et al, (26) and Biot have
 applied Lagrangian methods to the solution. Biot, et al use
 a two-dimensional width equation developed from Sneddon's
 equation modified to include Barenblatt's boundary condition
 to avoid infinite stress at the fracture tip (27). Wiles
 and Roegiers (28) apply a displacement continuity approach
 assuming linear elastic deformation under plane strain. By
 modeling the fracture as a series of short sections of arbi-

Clifton and Abou-Sayed (30) observed that fluid flow and elastic behavior of the rock primarily control fracture geometry. They note that fracture mechanics criteria affect only a small area at the fracture tip. Hence, they have developed a model which relates fracture geometry and height/length ratio to fluid flow and elastic deformation equations. The solution proceeds by calculating the stress field resulting from a pressure applied to the plane surface

Palmer and Carroll (29) present a similar model. Fracture width is calculated assuming two dimensional "line cracks" in vertical sections. These cracks correspond to the mathematical plane strain cracks described by England and Green (7). Width is related to height of each decoupled vertical section by an equation similar to that employed by Nordgren (16). Fracture height, for each vertical section, is determined by critical stress intensity factor. Fluid flow is assumed to be in one dimension along the fracture length. The model is reported by the authors to be applicable for fractures with a length/height ratio greater than five.

greater than those predicted by GCD type models. predicts fracture widths and net pressures approximately 30% shaped fracture in a non-uniform stress field. This model vary width the method is used to approximate an arbitrarily

In summary, most of the fracture design models currently in use rely on simplifying two-dimensional assumptions of fracture geometry. Usually fracture height is assumed based on gross formation thickness, or estimated using some functional relationship with fracture width, pumping time or some other parameter. The most commonly used equation relating fracture width and pressure is a form of Sneddon's equation which has been described previously (6). Recently Veatch has published a general overview of various commonly used fracture models (33).

refinement of fracture geometry calculations. most important factor studied. Little effort is spent on assume the GCD geometry. In this work, fluid leakoff is the the propagation of waterflood induced fractures. They also oretical interest. Hagort, et al (32) present a model for placement. The model is highly idealized and of little the- directed at design of hydraulic fractures through proppant the GCD type geometry in a fracture model which is primarily emphasis on other aspects of the problem. McLeod (31) uses Some simple fracture models have been presented with

gation. tained. A minimum width criterion controls fracture propa- Displacements generated by the stress field are then ob- of an infinite solid under conditions of zero shear stress.

force was published by J. Boussinesq in 1885. Timoshenko infinite half-space acted upon by a concentrated normal The solution for the displacement of the surface of an edge of the fracture will be described in more detail later. fracture. The boundary conditions applied at the leading tensile forces which prevent the continued extension of the ture, the half-spaces are assumed to be held together by is also applied. Outside the pressurized area of the frac- The condition of zero shear stress on the displaced planes where u is the displacement of one surface of a half-space. spaces. The width of the fracture, w , is thus given by $2u$, ing to deform or displace the surfaces of the two half- in the fracture is considered to be a distributed load act- the surface of a semi-infinite half-space. Fluid pressure Each face of the propagating fracture is assumed to be and England and Green (7).

sure is developed in a similar manner to that of Sneddon (6) gation. The equation used to relate fracture width to pres- ing a more fully three dimensional model of fracture propa- external control of fracture height is avoided, thus allow- assumptions required by earlier models. Most notably the described here is directed at eliminating some of the The model for hydraulic fracture propagation which is

NEW FORMULATION BASED ON CLASSICAL ELASTIC THEORIES

The distributed load is indicated by P_e , the radial distance from the point at which the deflection is calculated is S and ψ is the angle including the loaded element of area bounded by radii S and $S+dS$. These relations, as

$$u = \left[\frac{\pi E}{(1-\nu^2)} \right] P_e \iint d\psi dS \quad [16]$$

to be:

face of the plane, $z = 0$. The resultant equation is found displacement caused by point loads distributed over the surface of the plane is obtained by superposition of the displacement caused by a distributed load over a statically equivalent distributed load.

In this manner, the concentrated force is replaced by a face of a hemispherical depression located at the origin. concentrated force P is in reality distributed over the surface (force) is infinite. It must therefore be assumed that the displacement at the origin (point of application of the force) is the radial distance on the plane from the point of application of the force, P . Note that by this equation where r is the radial distance on the plane from the point

$$u_{(z=0)} = \frac{\pi E r}{(1-\nu^2)} P \quad [15]$$

0, caused by a concentrated load was found to be:
 load based on his work. The displacement of the plane, $z =$
 and Goodier (34) present the derivation for a distributed

applied to the current model, are derived in Appendix A. Note that if this equation is used to calculate the deflection at the center of a pressurized circle of radius r the result of integrating:

$$u = \left[\frac{\pi E}{2(1-\nu^2)} \right] p \int_0^r \int_0^{2\pi} d\psi ds \quad [17]$$

is:

$$u = \frac{E}{2(1-\nu^2)} p e r \quad [18]$$

which may be compared with Sneddon's equation (Eq. 1) with $y = 0$.

The general equation for the displacement of a point on the fracture surface (Eq. 16) is applied to a regular, square grid for which the value of the double integral can be analytically obtained. The behavior of the double integral influence function in space is discussed in more detail in Appendix A. Values of Poisson's Ratio and Young's Modulus are assigned to each square in the grid to allow simulation of a heterogeneous system. Net pressure on the fracture face at each block centered grid point is obtained by a coupled fluid flow calculation. To account for the variable properties a form of Eq. 16 suggested by Jaeger and Cook is used (35):

at any grid point requires a knowledge of the net pressure
 Calculation of the displacement of the fracture faces

Details of Mathematical Formulation:

in a later section.
 influence of the grid size effects are discussed in detail
 sized region is thus related to grid size. The magnitude and
 Barenblatt (8). In this model the length of the unpressur-
 imates that of the unpressurized fracture tip specified by
 characteristic strength of the rock. This condition approx-
 assumed to be tensile at all points and limited by some
 suit. The stress acting on the boundary block is, however,
 point other than the node center, a non zero value would re-
 of the displacement were calculated in a boundary block at a
 because of the nature of the formulation, if the magnitude
 placement of the node center is taken to be zero. However,
 At the boundary of the propagating fracture, the dis-
 each block center.

assumed constant within each grid block and are specified at
 homogeneous elastic medium. Values of ν , E , and P_e are
 determined for a variable pressure distributed over a heter-
 displacement of the fracture face at each grid point can be
 By making these approximations a value of the normal

$$u = \iint \left(\frac{\pi E}{(1-\nu^2)} \right) P_e d\psi ds \quad [19]$$

In a flowing, dynamic system, the fracture fluid pressure is related to the apparent fluid viscosity, flow rate, and fracture width at each point along the fracture. This leads to an iterative solution of fracture width and pressure. Assuming two-dimensional fluid flow in the x-y plane (with fracture displacements normal to this plane) the flowing pressure distribution is obtained by finite difference formulation. Details of the derivation of the fracture width equation are given in Appendix A. Derivation of the various terms are given in Appendix B. Briefly, fluid flow is assumed to be laminar between parallel fracture walls. With Willis (37).

of the least principal earth stress as shown by Hubbert and the plane of the numerical grid, is normal to the direction It is assumed that the plane of the fracture, which is also

flowing equation (36).
$$P_e = P_f - \sigma - P_p$$
 [20]

the pore pressure in a permeable rock bed, P_p , by the following the fracture, P_f , the least principal earth stress, σ , and a fracture face is related to the total fluid pressure in fined the net or effective pressure causing displacement of applied to the fracture face at that point. As usually de-

$$\Delta p = P_e - (\sigma - \alpha p)$$

these assumptions, the volumetric flow rate, Q , can be obtained by:

$$Q = \left[\frac{12 \mu_a}{h} \right] \frac{d\alpha}{d} (P + \gamma h)^w \quad [21]$$

where h is the length of a grid block normal to the direc-

tion of flow, μ_a is the apparent viscosity of the fluid, γ

is the potential gradient or gravity head, and w is the

fracture width. For flow between two nodes of different

widths, the harmonic average of the cube of the widths is

used. The derivation of the working pressure equation, pre-

sented in Appendix B, proceeds from a material balance writ-

ten on each fracture node as:

$$\sum q_{in} - \sum q_{out} + q_{inj} - q_{loss} = Acc. \quad [22]$$

The accumulation term in the equation accounts for both

compression of the fracturing fluid, assuming slightly com-

pressible fluid, and change in the volume of the fracture.

The final working equation relating pressure and width is

written as:

$$T_{j, j-1}^{i, j} P_{i, j-1}^{i, j} + T_{i, j}^{i, j} - \left[T_{i, j}^{i, j} + T_{i, j}^{i, j} + T_{i+1, j}^{i, j} + T_{i, j+1}^{i, j} \right] P_{i, j+1}^{i, j} =$$

$$\left(\frac{\partial a}{\partial t} \right) \left\{ \left[\int \int \frac{\pi E}{(1-\nu)^2} d\psi ds + u_k^c \right] (p_{i,j}^{n+1} - p_{i,j}^n) - \left(TI_{i,j}^{\gamma a} + TI_{i+1,j}^{\gamma a} - q_{in}^i + q_{loss}^i \right) \right\} \quad [23]$$

The volume of fluid contained in each node is expressed in terms of the fracture half-width at the previous, known iteration level, u_k . The transmissibilities in the i and j directions are defined as, for example:

$$TI_{i,j} = \left[\frac{4.5984 \times 10^{-6}}{3} \frac{u_a}{w_{i-1/2,j}} \right] \quad [24]$$

where the apparent fluid viscosity, μ_a , can be determined for Newtonian or non-Newtonian fluid. The harmonic average width cubed is calculated from:

$$w_3^{i-1/2,j} = 2 \left[\frac{u_{i-1,j}^3 * u_{i,j}^3}{u_{i-1,j}^3 + u_{i,j}^3} \right] \quad [25]$$

The fluid leakoff rate, q_{loss} , from each node is estimated using fracture fluid leakoff coefficients defined by Howard and Fast (17). In the present formulation wall building fluids are not considered, hence the total leakoff coefficient is given by:

$$C_I = \frac{C_{II}^I + C_{II}^I}{C_{II}^I * C_{II}^I} \quad [26]$$

This form is derived directly by differentiating the width equation (Eq. 16) with respect to pressure. The approximation, which assumes that $\frac{\partial P}{\partial t}$ is equal at all nodes, is necessary to allow a tractable solution of the problem. The approximation can be improved by relating the actual ΔP dis-

$$[30] \quad \frac{\partial P}{\partial w} = \iint \frac{\pi E}{(1-\nu)^2} d\psi ds$$

is:

The change in fracture width with respect to pressure

in units of ft³/sec.

$$[29] \quad q_{loss\ i,j} = \frac{60 \sqrt{\tau}}{C_{T\ a}^2}$$

rate is:

Units of the fracturing fluid loss coefficients are ft/(min)^{1/2}. Considering a node with an area of a^2 which has been exposed to fracturing fluid for a time, τ , in minutes (the time since that node opened), the fluid loss

$$[28] \quad C_{II} = 0.0374 \Delta P \sqrt{\frac{K\phi c_r}{n}}$$

and

$$[27] \quad C_I = 0.0469 \sqrt{\frac{K\Delta P\phi}{n}}$$

where

Injection rates adds up to the total specified rate. subject to the condition that the sum of all individual node

$$[32] \quad q_{inj,1}^b = \left[\frac{q_a}{9.1968 \times 10^6} \right]_{n,1}^3 \Delta P^w,$$

The injection rate into each node is then given by:

$$[31] \quad \Delta P^w = \frac{q_{HI}}{2} \left[\frac{q_a}{9.1968 \times 10^6} \right]_{n,1}^3$$

node center is defined by:
 conditions. The pressure drop between the wellbore and the more rigorous approximation may be necessary under some conditions. A flows freely through the perforations to the node center. For a perforated well completion, this assumes that fluid This approximation is applicable for open hole completions. between the wellbore fluid and each fracture node center. missibility of each node assuming a constant pressure drop the open nodes. Partitioning is done on the basis of trans- jecton rate into one wing of the fracture, Q_{HI} , between wellbore is obtained by partitioning the total specified in- The injection rate term for each node adjacent to the term accounts for compression of the fluid in the fracture. length/height ratios. The remainder of the accumulation been found satisfactory for most cases except very high, tribution to the derivative. The current approximation has

Equation 23 is written for each open node in the fracture grid, where fluid flow is taking place. Solution of the resulting five-diagonal matrix yields values of the node pressures at the advanced time level. The effective stress on the walls of the fracture at each block center is calculated using Eq. 20.

$$\sum_b \left[\iint \frac{\pi E}{(1-\nu^2)} p \, d\psi \, ds \right]_b = - \sum_f \left[\iint \frac{\pi E}{(1-\nu^2)} p \, d\psi \, ds \right]_f \quad [33]$$

Grid blocks comprising the boundary of the fracture are defined to have a fracture width, at the node center, equal to zero. The displacement at each node center is influenced, according to Eq. 19, by all node center pressures obtained by solution of the matrix resulting from Eq. 23. However, each node displacement is also related to the tensile stress established in each of the boundary nodes. To assure a zero displacement at all boundary nodes, a simultaneous solution for all boundary stresses must be made. An equation, of the form:

Grid blocks comprising the boundary of the fracture are defined to have a fracture width, at the node center, equal to zero. The displacement at each node center is influenced, according to Eq. 19, by all node center pressures obtained by solution of the matrix resulting from Eq. 23. However, each node displacement is also related to the tensile stress established in each of the boundary nodes. To assure a zero displacement at all boundary nodes, a simultaneous solution for all boundary stresses must be made. An equation, of the form:

Calculation rate into each node open to the wellbore. Calculate the values and the latest iterative estimate of fracture width at each node to calculate transmissibilities. Calculate the est estimate of shear rate in each fracture node. Use these Calculate all apparent fluid viscosities from the lat-

ing the required calculation for a timestep is as follows:
is begun. In brief, the logic sequence involved in complet- and old timestep values are updated and a new timestep loop and no fracture extensions are required, all time counters, stable fracture size results from the iteration procedure, width and the entire iteration procedure is repeated. If a ture propagates are assigned an arbitrary, small fracture is extended into that node. All nodes into which the frac- specified strength of the material at that node the fracture tip, if any boundary node tensile stress exceeds the amount of tensile stress which can be applied at the frac- Assuming that the material tensile strength limits the of great importance in fracturing laboratory scale samples.

Fairhurst (39) have shown that material tensile strength is sion must be resisted by some tensile strength. Haimson and pagation criterion (36-39). Most feel that fracture exten- sed the use of material tensile strength as a fracture pro- tured material exist (14). Other authors have also discus- no stresses greater than the tensile strength of the frac-

late fluid loss rates for each open fracture node. Using all these parameters, calculate the flowing fracture fluid pressures in each node. Solve for boundary stresses such that the fracture width at the boundary is zero. Using all the boundary node stresses and fluid pressures, recalculate fracture widths. Iterate until fracture widths and pressures converge. Check all boundary node stresses and extend the fracture into those with tensile stresses greater than the specified tensile strength of the material. If fracture nodes are extended, recalculate the timestep. If a stable fracture shape results, increment time counters and continue with next timestep.

Some fluctuation in fracture shape occurs immediately following fracture extension. Because of material balance constraints, the fracture width at all existing nodes decreases when a new grid block is fractured. Subsequent injection tends to re-inflate the model fracture before another set of grid blocks fractures. The arrays of calculated fracture widths, pressures, and rock stresses are only output for timesteps immediately preceding the extension of a fracture. By only writing timestep output at these times a more consistent picture of the fracture extension process is generated.

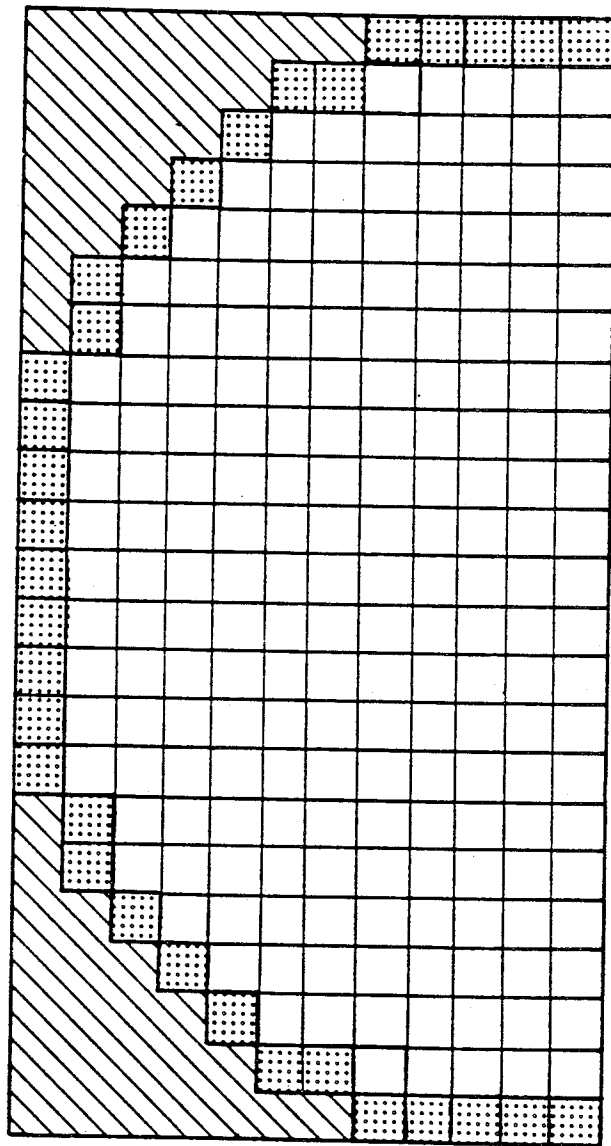
To compare the magnitude and distribution of fracture widths obtained using the current model with those generated by Sneddon's equation, a grid modeling a circular fracture under conditions of constant pressure was used. The grid, shown in Figure 1, was composed of ten foot square blocks. The stippled grid blocks comprise the boundary of the frac-

Equation:
Comparison of Fracture Width Prediction With Sneddon's

ted in this and later chapters. calculations and comparisons for both programs are presented in effective stresses and elastic properties. Sample It also shows the effects on fracture shape of various current formulation with classical fracture geometry theories also calculated. This model is useful for comparison of the boundary stresses at the specified edges of the fracture are distribution for any specified static pressure distribution. simpler program allows the calculation of a fracture width fracture in a heterogeneous elastic medium. The second, injection of a viscous fracturing fluid, of a hydraulic model. It is useful in predicting the growth, during plies the dynamic fluid flow equation with the fracture geometry model. One model cou- the derivations presented in the Appendices. One model cou- Two separate computer programs were written based on

RESULTS OF STATIC MODEL CALCULATIONS

Figure 1. Grid Used to Model a Radially Symmetric Pressurized Fracture



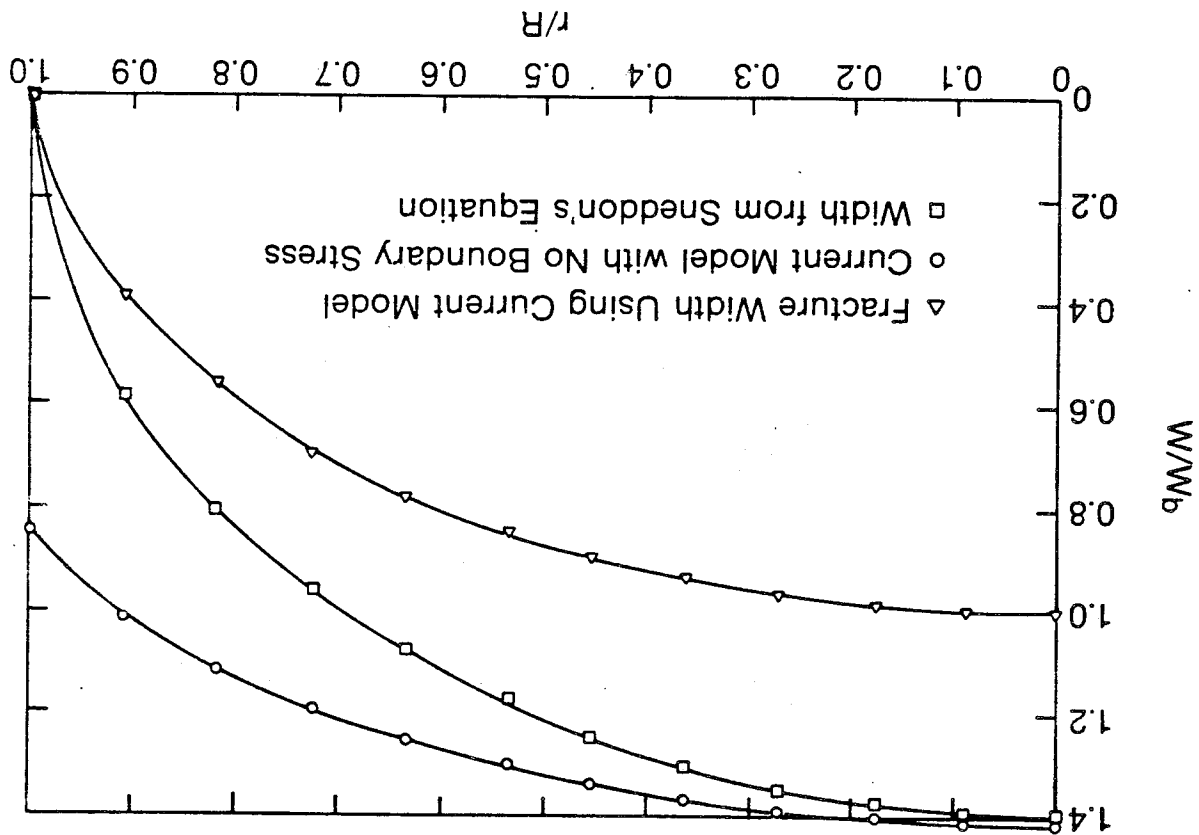
The plots of the normalized displacements (Fig. 2) show the relationship between the various methods of calculating

$$u = \frac{E}{2(1-\nu^2)} \Delta P \sqrt{R^2 - r^2} \quad (34)$$

tion (6). The fracture half-widths obtained from the model are normalized and plotted in Figure 2. The width at the center of the fracture is normalized to 1.0. Normal displacements of the fracture face, neglecting the effects of the boundary node stresses, are also plotted. These results are compared with displacements obtained using a form of Sneddon's equation (6).

The fracture half-widths obtained from the model are element on calculated fracture widths. The calculation procedure includes the effect of the other half of the semicircular symmetry dynamic growth studies. The calculation procedure includes strength is only used as a fracture extension criterion in values are not assigned in the static model cases. Tensile psi is applied to the fracture face. Tensile strength value of 3.0×10^6 psi. A constant effective stress of 1000 ratio is assigned a value of 0.2, and Young's Modulus a grid blocks high and eleven wide at the center. Poisson's The pressurized area of the model fracture is twenty-one procedure because it lies outside the fracture boundary. The hatched area is not considered in the calculation

Figure 2. Normalized Fracture Width Versus Radius For A Symmetric, Constant Pressure, Circular Fracture



Fracture width. Sneddon's equation yields a fracture width nearly equal to that predicted by the current formulation, when boundary stresses are ignored. When the boundary stresses are included, the width at the fracture center is reduced. Under these conditions Sneddon's equation predicts a width at the fracture center approximately 1.4 times that given by the model. Observations of the forms of the equations used justifies the relationship between the results of Sneddon's equation and the unbounded model. As shown in the earlier discussion (Eqs. 16-18), the current model equation, when directly integrated for a radially symmetric crack, yields an analytical solution for the displacement at the center of the crack which is equal to that given by Sneddon. This indicates that the influence of stresses at the fracture boundary on the width at the crack center are given much less weight in Sneddon's width equation than in the present model. The current model does, however, predict the approximately elliptical fracture shape which is classically assumed (2-7). Further, an analysis of grid size effects, which is presented in detail later, indicates that as node size approaches zero the current model converges to the analytical solution given by Sneddon. This procedure generates a tensile stress at the fracture boundary which approaches infinity. The current model solution, with the

The other commonly assumed geometry (GGD model) applies the width equation to ellipses in the horizontal plane. At any point along the length of the crack, the vertical fracture walls are assumed to be parallel. Thus, a state of plane strain is assumed in horizontal planes normal to the fracture plane. This type of model predicts a fracture width, at the wellbore, which will grow, under constant pressure, with fracture length. Boundary or confining ef-

along a vertical cross-section is determined. The width distribution and internal pressure, the width distribution of pressurized fracture length. For a given fracture height and internal pressure, the width distribution of these assumptions, the fracture width is found to be independent of pressurized fracture length. As a result vertical planes normal to the fracture plane. These models presume that a state of plane strain exists in elliptical cross-sections in the vertical plane (13-16). (Eq. 1). The PKN type models apply the width equation to essentially similar in form and theory to Sneddon's equation models are based on various equations (Eq. 3,5), which are As discussed earlier, the most commonly used fracture

Comparison of Current Model With Previous Models for Various Fracture Length/Height Ratios:

illustrated. applicable, especially for non-circular fractures as will be realistic distributed tensile stresses obtained, may be more

Several test cases were run with varying ratios of fracture half length to half height. A ratio of 1.0 indicates an approximately radially symmetric fracture. A constant fracture half-height of 50 ft. was maintained while

These data comprise the "base case" used for all comparison studies.

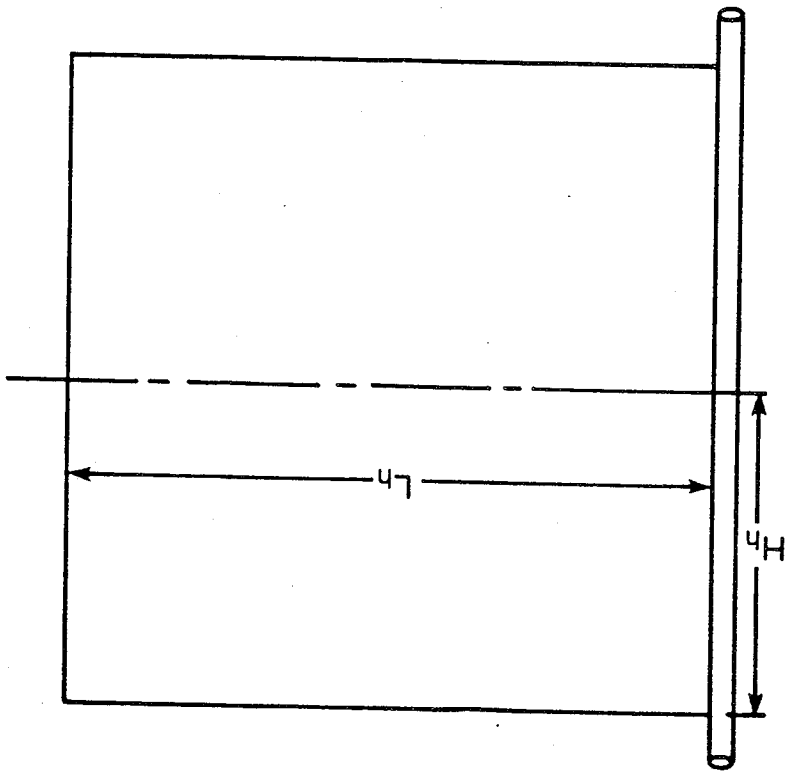
$$\begin{aligned}
 \nu &= 0.2 \\
 E &= 3 \times 10^6 \text{ psi} \\
 P_e &= 1000 \text{ psi} \\
 a &= 10 \text{ ft.}
 \end{aligned}$$

[35]

low, were used. rock elastic properties and pressures, which are given below, were used. Symmetry about the wellbore is assumed. Constant rectangular fracture, whose geometry is shown in Figure 3, between these models and the current formulation, a model short fractures ($L/H < 1.0$). To investigate the relation GGD geometry has been presented as applicable for high, height ratios much larger than one (18,19). Likewise, the are applicable for low, long fractures, i.e., length to Several authors have stated that the PKN type models ding planes at the upper and lower fracture extremities. The walls of the fracture are assumed to slip along the bed-facts at the upper and lower fracture edges are ignored.

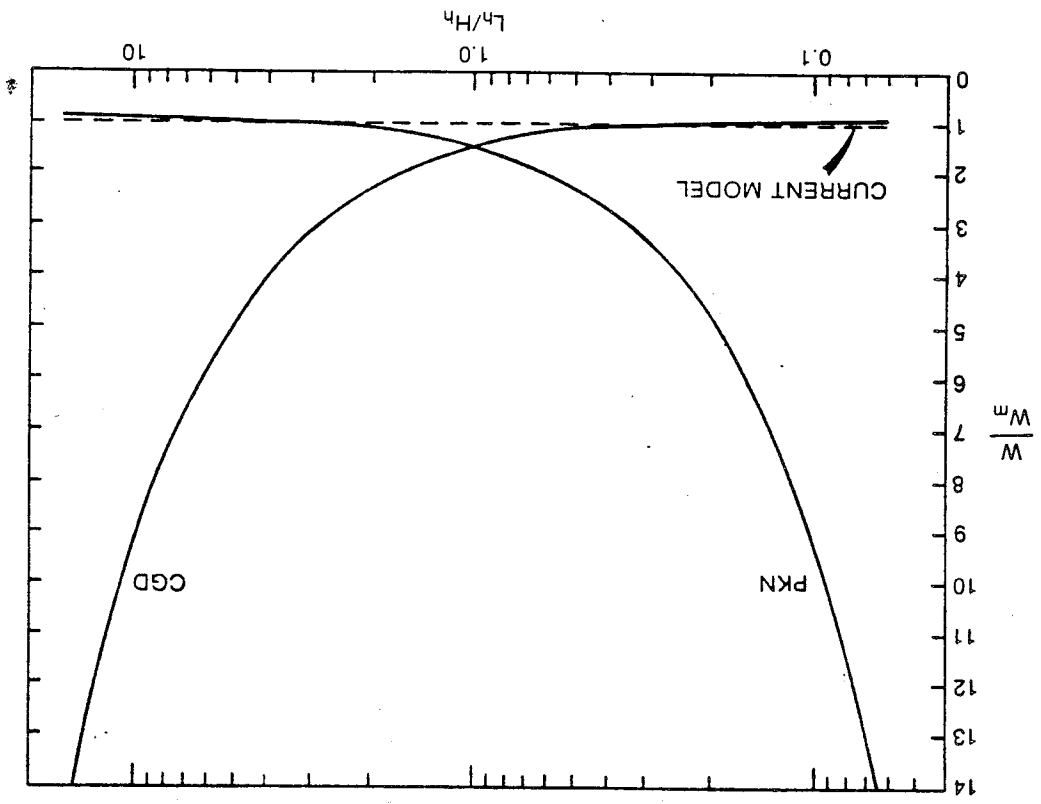
UNIVERSITY OF MICHIGAN LIBRARY

Figure 3. Schematic of Model Fracture Showing Principal Dimensions for Comparison with Classical Width Equations.



UNIVERSITY MICROFILMS

Figure 4. Fracture Widths Obtained from PKN, CGD, and Current Models for Various Fracture Aspect Ratios.



UNIVERSITY OF MICHIGAN LIBRARY

ter of the fracture is independent of position along the fracture length. The GCD type models predict an elliptical distribution of fracture width with position along the fracture length, for any assumed fracture height or length. Using results from the current model obtained in generating Table 1, a series of plots of normalized fracture width versus normalized fracture length (w/L) can be generated for various values of L/H . Figure 5 is comprised of these plots for aspect ratios (L/H) of 0.24, 0.90, 4.1, and 12.1. The data show that for aspect ratios less than one, the normalized widths follow a roughly elliptical curve. In ratio's larger than one, the width behaves as though it were independent of position over part of the fracture length. The widths for all aspect ratio's converge smoothly to zero at the fracture edge. These cases show that for a fracture of assumed constant height, under constant internal pressure, the current model predicts fracture widths which behave in a similar manner to the applicable classical fracture model. That is, widths approach those given by PKN models for L/H greater than one, and GCD models for L/H less than one.

The comparison cases presented also indicate that, under proper conditions, the classical models yield an estimate of fracture geometry similar to that obtained with the

46

UNIVERSITY OF MICHIGAN LIBRARY

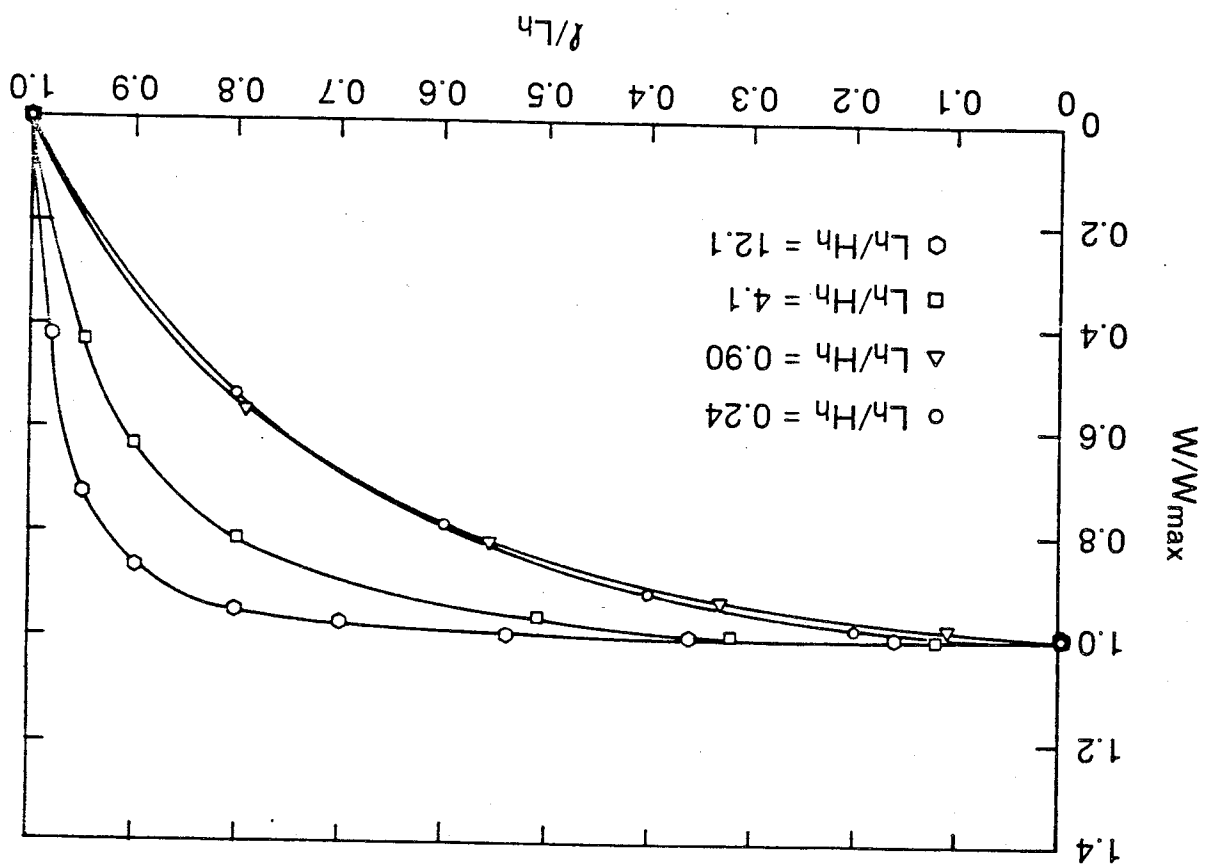
UNIVERSITY OF MICHIGAN LIBRARY

TABLE 1

$T_1 h/H_1 h$	W_{T_1}/W (GPD)	$W_{h/W}$ (PKN)
0.0621	0.912	14.67
0.0826	0.922	11.15
0.1235	0.938	7.60
0.2439	0.985	4.03
0.4762	1.09	2.29
0.5000	1.13	2.25
0.7692	1.28	1.66
0.900	1.39	1.55
1.111	1.55	1.39
1.30	1.66	1.28
2.0	2.25	1.11
2.1	2.29	1.09
4.1	4.03	0.985
8.1	7.60	0.938
12.1	11.15	0.922
16.1	14.67	0.912

Table 1: Fracture widths obtained by GPD and PKN width equations normalized to current model predictions for various length/height ratios.

Figure 5. Normalized Width Versus Normalized Length Profiles for Various Length/Height Ratios

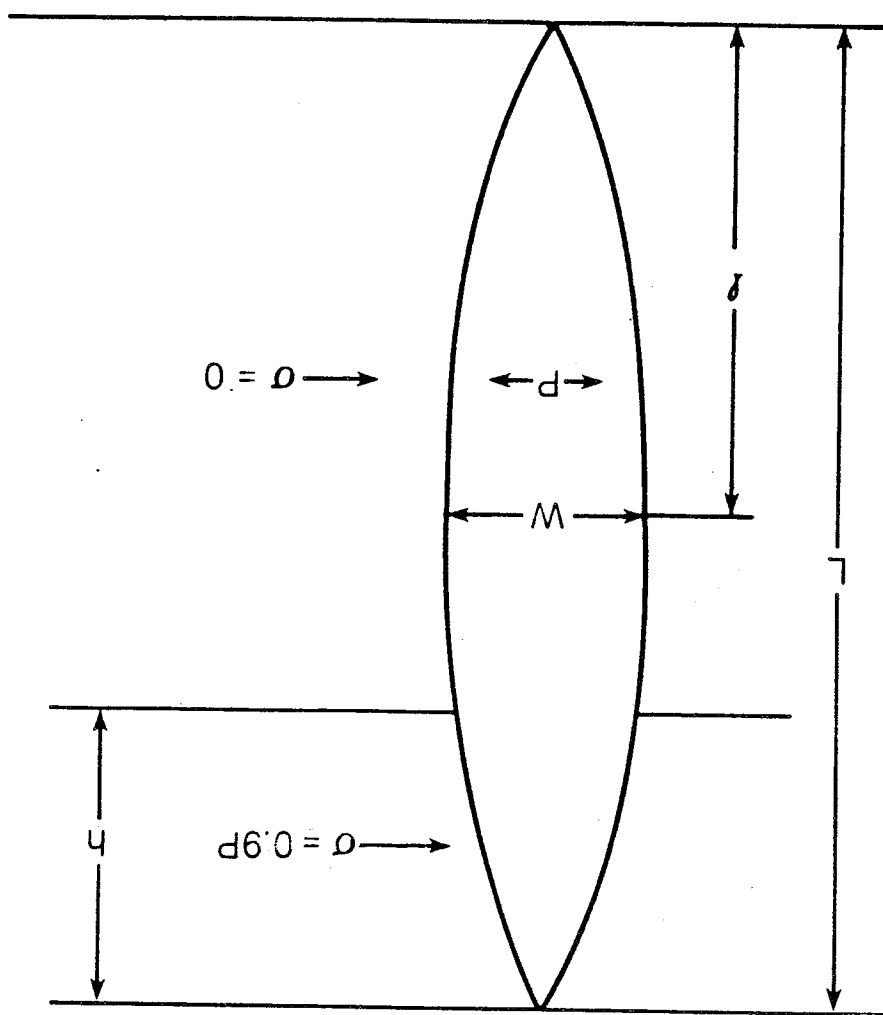


One of the advantages of the current model over most existing models is its ability to predict fracture geometries in heterogeneous elastic media, or non-uniform stress fields. Hanson, et al (40), used a boundary element model, derived for plane-strain conditions to estimate fracture geometries in layered systems. A hydraulic fracture of length, L , was assumed to extend for some part of its height, h , into a layer of high confining stress. The assumed geometry is shown in Figure 6. The high confining stress layer was assigned a stress value of 0.9 times the pressure in the fracture. This can also be modeled by changing the net pressure on the fracture walls. Using this geometry with an aspect ratio of 1.0, a set of simulations was conducted for various depths of penetration of the fracture into the high stress layer. Calculated widths along the central axis of the fracture were normalized to the maximum fracture width, under uniform stress conditions,

Effects of Variations of Elastic Properties and Confining Stresses on Calculated Fracture Widths:

control which is not required in the current model. Thus all results are dependent upon an external height. Thus all results are dependent upon an external approaches depend strongly on an assumed value of fracture that the simple geometries modeled by the classical current formulation. It is important to remember, however,

Figure 6. Assumed Geometry for Confining Stress Variation Study, After Hansen, et al (40).



and plotted as a function of normalized fracture length. These data (Figure 7) show that a high confining stress or low effective pressure in the fracture causes a resultant decrease in widths over a part of the fracture length. For shallow penetration into the high stress layer, $h/L = 0.1$, the width over most of the fracture is only slightly affected. At a penetration depth equal to half the fracture length, the maximum width is decreased to about 72% of its value under homogeneous stress. Also, the position of the maximum width is shifted from the center of the fracture to about one third of the length of the fracture from the un-stressed tip. These results are in excellent agreement with the data presented by Hanson, et al (40).

The effects of variations in elastic properties may also be studied using the geometry described by Figure 5. A series of fracture geometries were studied for various depths of penetration into a layer of higher Young's Modulus (7×10^6 psi compared with 3×10^6 psi). The results (Figure 8) show the same trends as for a higher confining stress layer. In these studies, the net stress over the entire fracture was maintained as a constant. In a natural, layered rock medium, it is important to consider both the variation in elastic properties and their effects on the in-situ stress field (40).

Figure 7. Normalized Fracture Width versus Normalized Length for Various Depths of Penetration into a High Confining Stress Layer.

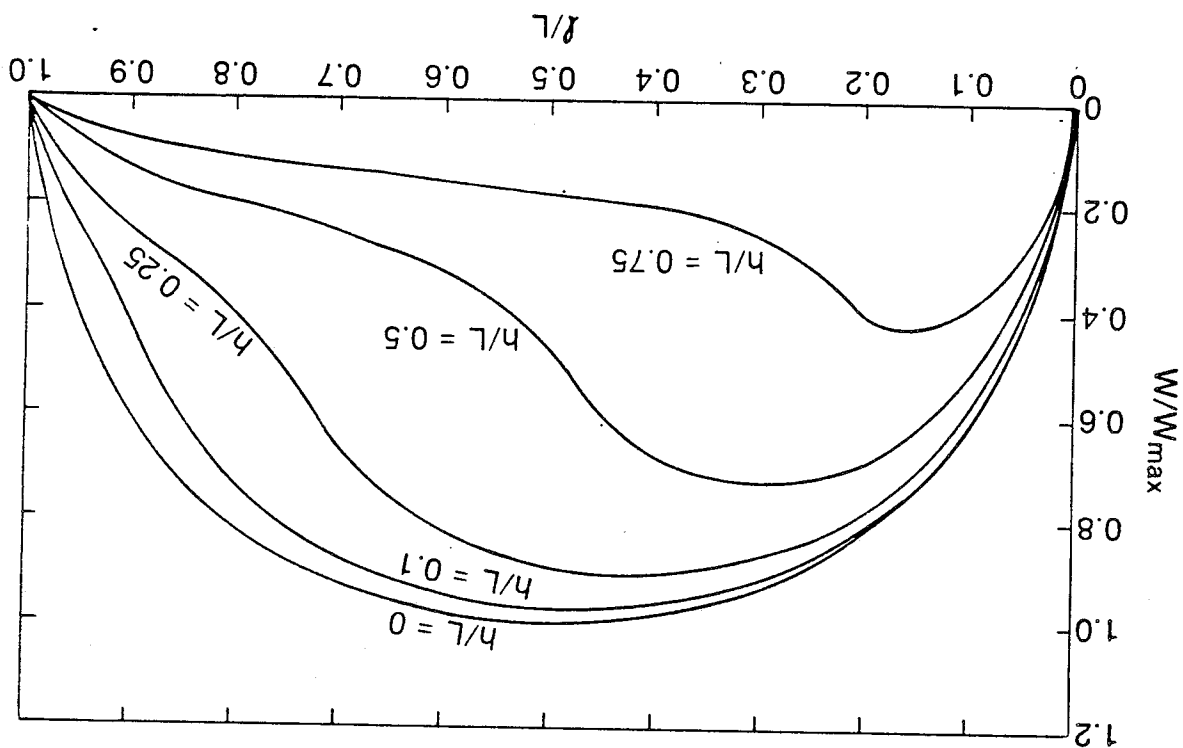
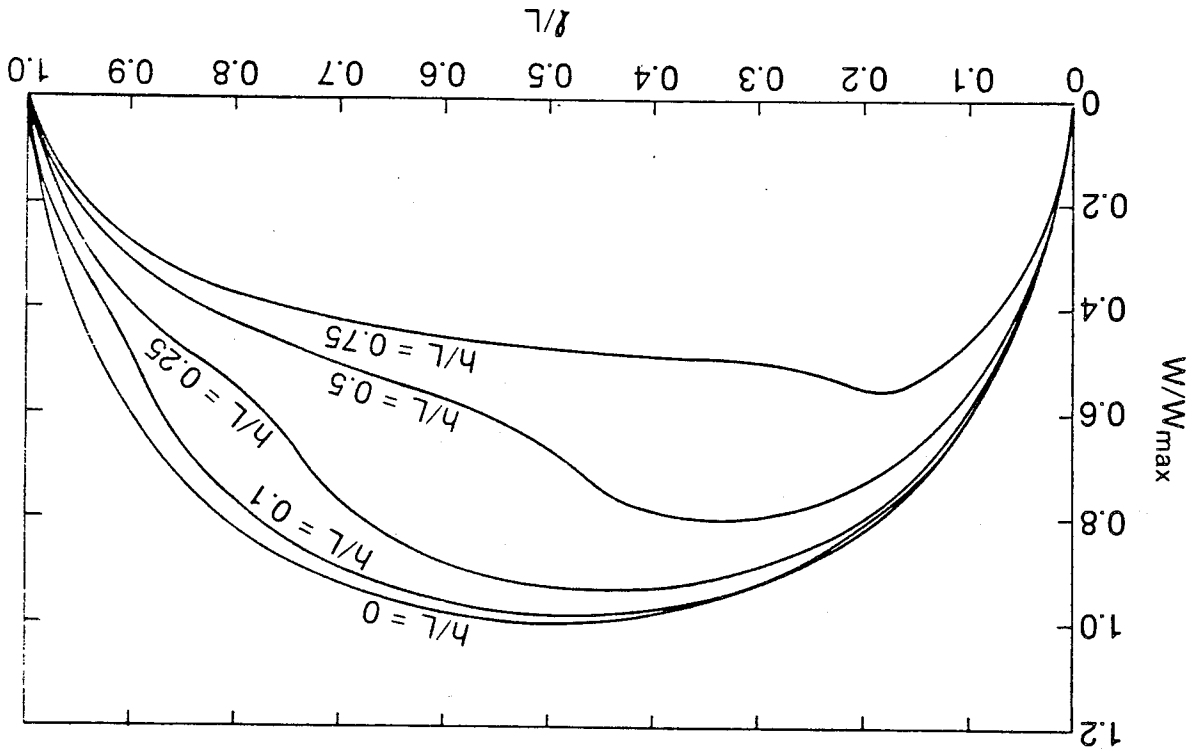
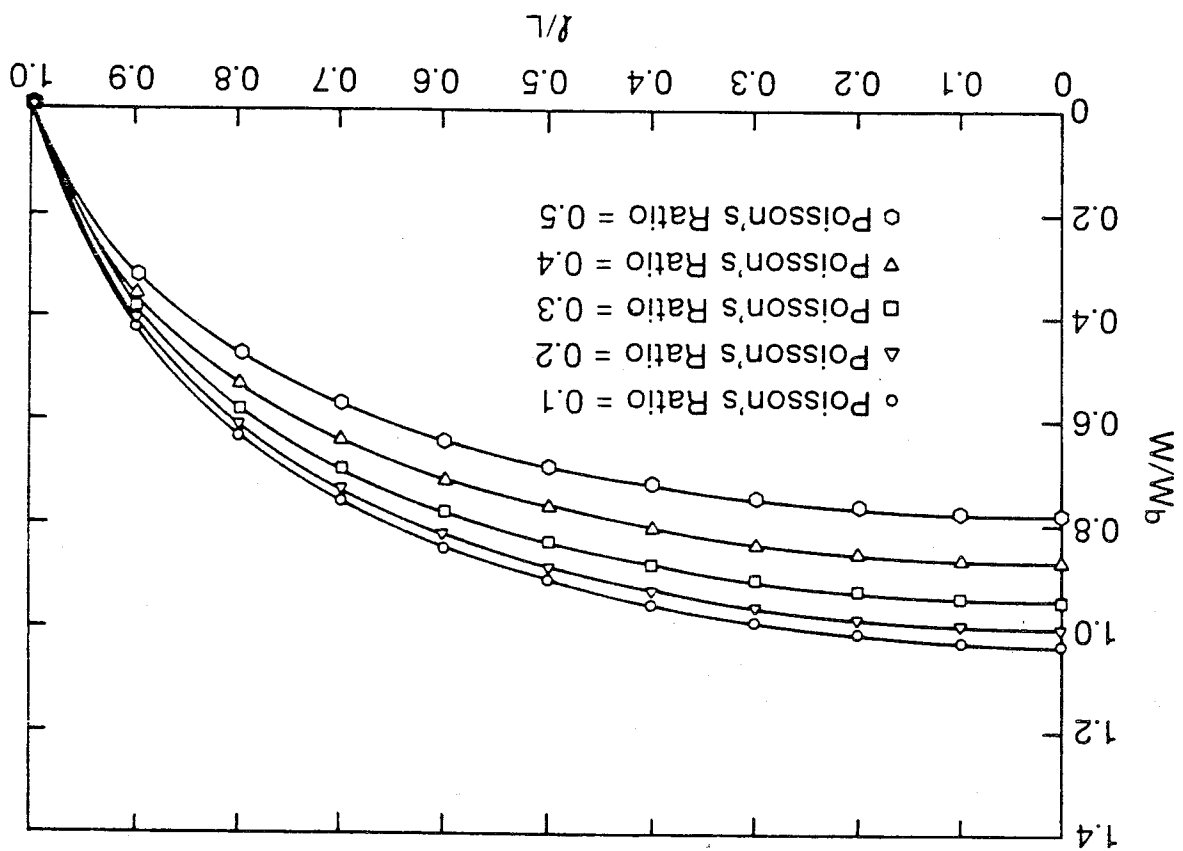


Figure 8. Effect on Fracture Width of Partial Penetration Into a Layer of Higher Young's Modulus.



width. These cases indicate that the principal physical parameters affecting fracture geometry are first, confining stress variations in rock systems, and secondly variations in material moduli. Poisson's Ratio was found to have little direct effect on fracture shape. However, it is possible that this parameter could significantly affect in-situ stress values which can affect fracture shape. A distinction should also be made between fracture geometry, in the context used here, and fracture containment. Containment is a dynamic, propagating effect and cannot be studied with a static model. Effects of parameters on fracture containment must be analyzed using the fully dynamic fracture growth model coupling fluid flow with the elastic rock deformation.

Variations in Poisson's Ratio were found to have much less effect on fracture geometry. Figure 9 is a plot of normalized width along the fracture half-length for various values of ν . Because of the small effect, Poisson's Ratio was varied over the entire fracture grid for these cases. Over the most common range of values for reservoir rocks, 0.1 to 0.3, the variation in the maximum fracture width was found to be less than six percent of the base case ($\nu = 0.2$).



Another effect which can be studied using the static fracture geometry model is that of node size on calculated geometry. As node size decreases, the negative contribution to displacement at any point in the fracture caused by tensile stresses in the boundary nodes should decrease. To quantify this effect, a static fracture grid with a height of 60 feet and a half-length of approximately 90 feet was used. The fracture grid was subdivided into nodes of 5, 10, and 15 feet for three different geometry calculations. The same constant stresses and rock properties were used for all cases. Figure 10 is a plot of fracture width, normalized to the base case discussed previously (with a node size of ten feet), at various positions along the fracture length. The maximum fracture width at the wellbore, from the base case, was used as the base for normalization. Approximately a ten percent error is introduced in the maximum calculated width at the fracture center for these variations in node size. This difference is related to the relative sizes of the areas occupied by the boundary nodes, with their calculated negative stresses, and the pressurized fracture. As the ratio of the area occupied by the boundary nodes (A_b) to the area occupied by the fracture (A_f) approaches zero the

Effects of Grid Size on Fracture Geometry:

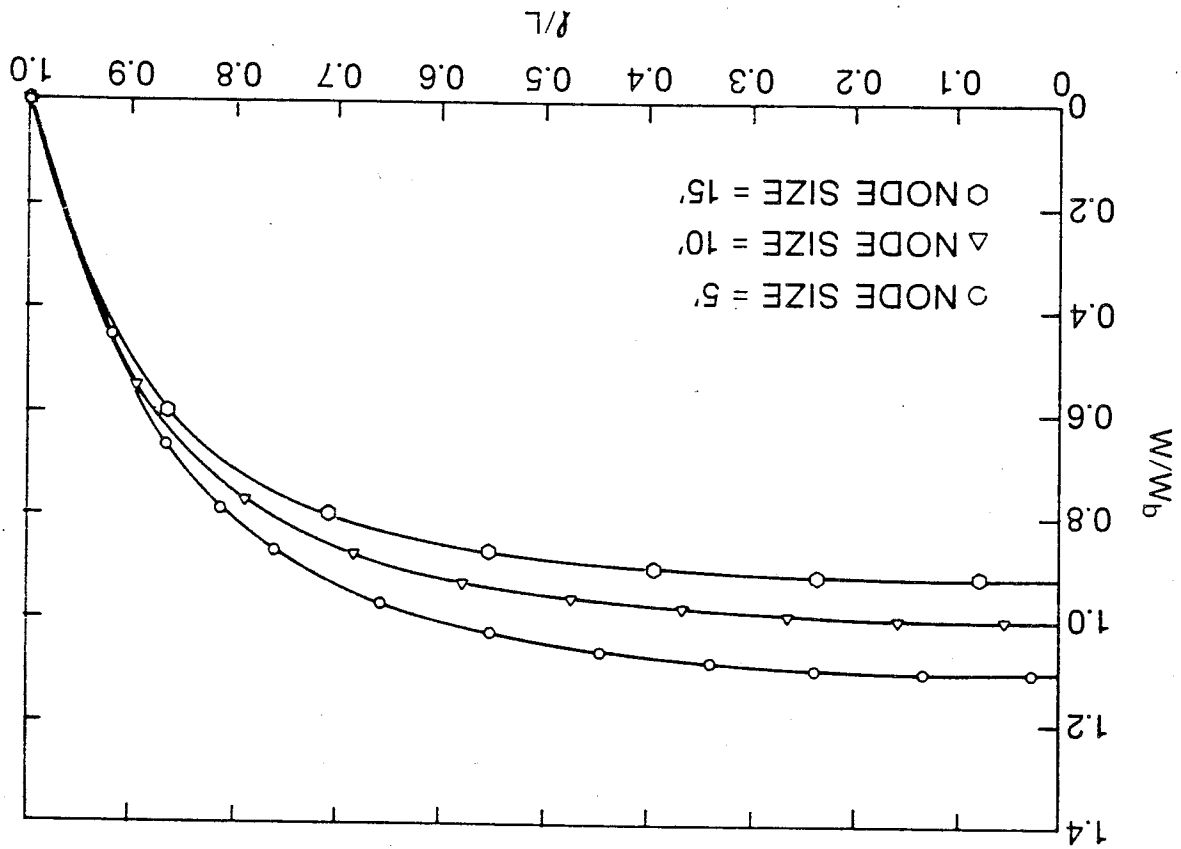


Figure 10. Effect of Node Size on Calculated Fracture Geometry

calculated width approaches the analytical solution given by Sneddon. Figure 11 is a plot of width, normalized to the base case (10 ft. node) for various area ratios. The extension of the line to approximately 1.39 is justified by the data in Table 1 comparing the Sneddon equation with the current model for an L/H value of approximately 1.0.

As the area occupied by the fracture boundary decreases, each boundary node must sustain a higher tensile stress to maintain the zero displacement condition if only one row of boundary nodes is used. As the area of a boundary node approaches zero, the stress required must correspondingly approach infinity. This trend is shown in Figure 12 which is a plot of boundary node stress versus the relative area of fracture boundary. The boundary stress is plotted as a multiple of the constant effective fracture fluid pressure. The trend at high ratios ($A_p/A_f \approx 1.0$) indicates that as the boundary area increases the required boundary stress approaches the effective fracture fluid pressure. These observations of the effects of node size indicate that the current model will converge to the results obtained by Sneddon under the conditions he defined, i.e., a zero thickness fracture boundary, with infinite tensile stress. For small node sizes, this unrealistic stress condition can be avoided by inclusion of more than one layer of boundary nodes.

Figure 11. Effect of Ratio of Boundary Area to Fracture Area on Calculated Fracture Widths

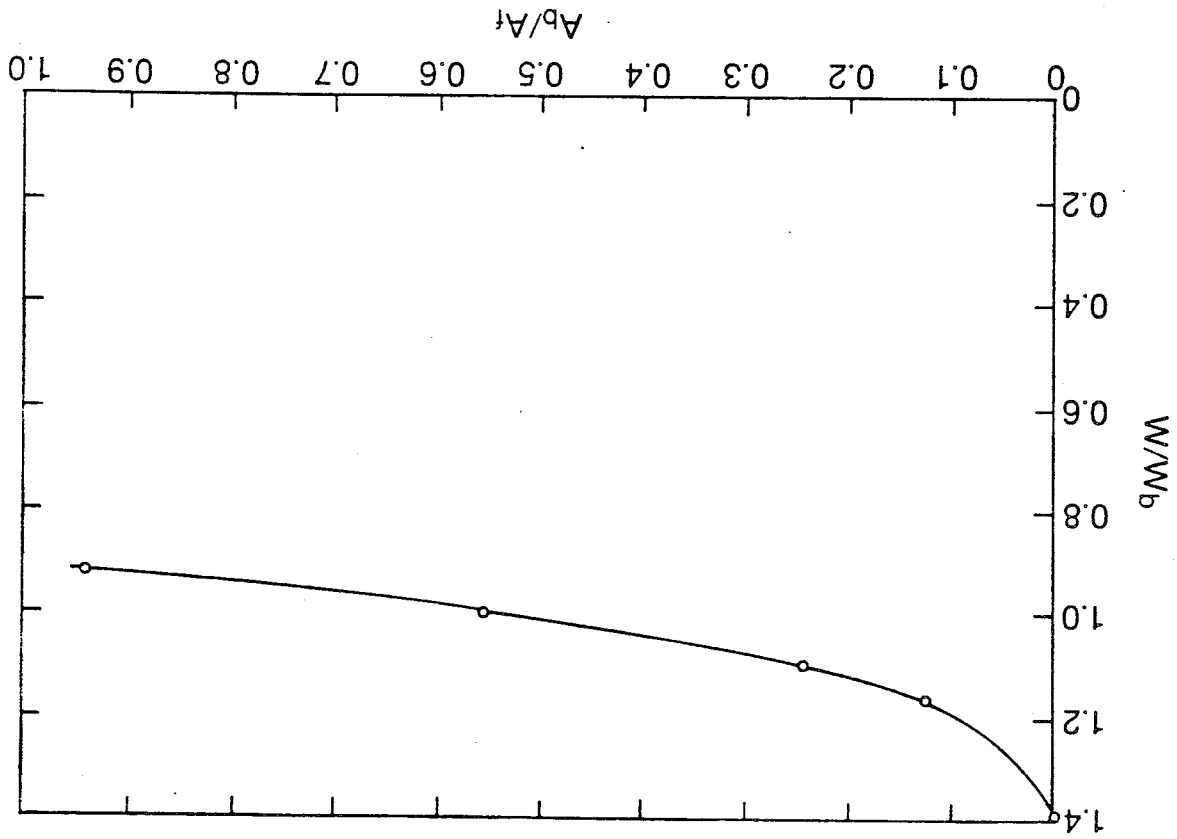
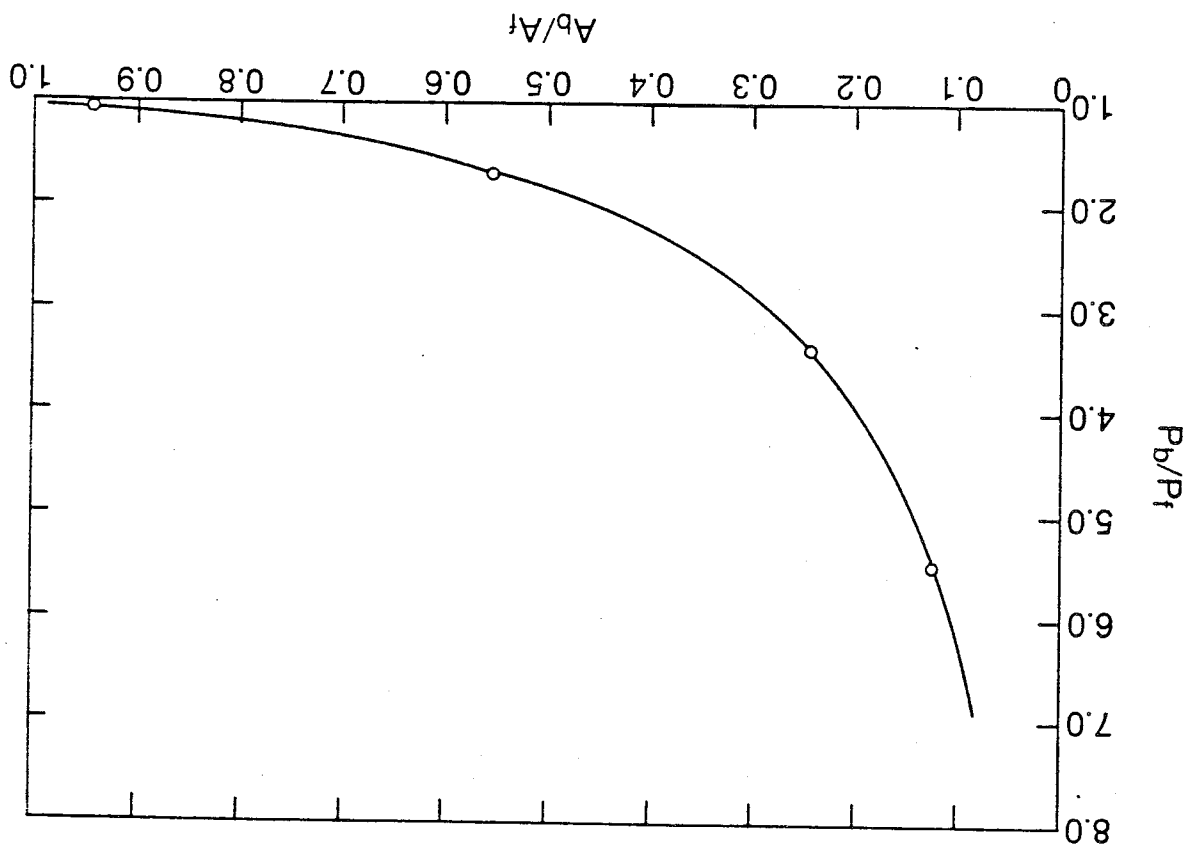


Figure 12. Increase in Boundary Node Stress For Various Relative Magnitudes of Fracture Boundary and Pressurized Fracture.



where T is the allowed maximum tensile stress in the material and R is a characteristic fracture length. Investigation using the current model indicates that this relationship is useful for selecting node size when the larger of the fracture half-length or half-height is used for R . In general, when a constant node size is used, the boundary effects cause an underestimation of fracture width at early times during the fracturing process. It should be noted that this underestimation is a result of discretization of the process rather than an error in the model formulation.

$$\Delta s = R \left[\frac{1 - \sqrt{1 - \frac{P}{P+T}}}{1} - 1 \right] \quad [36]$$

node, is related to the fracture half-length by: zone, which is modeled here by the width of the boundary and Krech suggest that the length of the stressed boundary intermediate or changing value must be selected. Perkins ary and fracture changes throughout a simulation run, an ary area. However, because the ratio of areas of the bound-upon selection of an applicable node size or width of bound- Accurate application of the current model is dependent

$$|\epsilon| < 1,$$

As presented in Eq. 23, the formulation for the pressure equation based on fluid flow within the fracture is implicit with respect to pressure. Applying the standard Von Neumann analysis for stability of an implicit finite difference formulation (41), it can be shown that the error term at any point in space and time will not increase, hence the solution will be stable, as long as:

Discussion of the Numerical Stability of the Dynamic Model:

Test cases are presented which address the computational stability of the dynamic growth model of a well confined vertical fracture is compared to the analytical solution presented by Nordgren (Eqs. 8,9). Time requirements and iteration counts are also presented for a simple well-defined fracture geometry.

The computer program to carry out the calculations comprising the model described here is written in standard FORTRAN. The program consists of 1627 records. Test cases described here were run on a Burrough's R7900 computer at Marathon Oil Company's Denver Research Center. Matrix solution packages used in the simulator were obtained from the IMSL library.

NUMERICAL CHARACTERISTICS OF DYNAMIC PROPAGATION MODEL

The geometry selected for the stability analysis is a well-confined vertical fracture of constant height, which conforms to the geometrical assumptions made by Nordgren. The analytical solution presented by Nordgren (16) is used as a check on convergence of the current formulation. A reservoir simulator.

This number is similar in form to the Courant number which is commonly used as a measure of stability for numerical

$$D = \frac{Q \Delta t}{w \Delta x^2} \quad [40]$$

formulation, several test cases were run on a single fracture geometry for various values of the dimensionless group. To demonstrate the range of stability and convergence of the current evaluation of transmissibilities which are functions of pressure, some additional instabilities may arise. Because of the dependence of the pressure solution on formulation is unconditionally stable.

value of $|\xi|$ is always less than or equal to one, and the is positive for all positive values of Δt and Δx . Thus, the

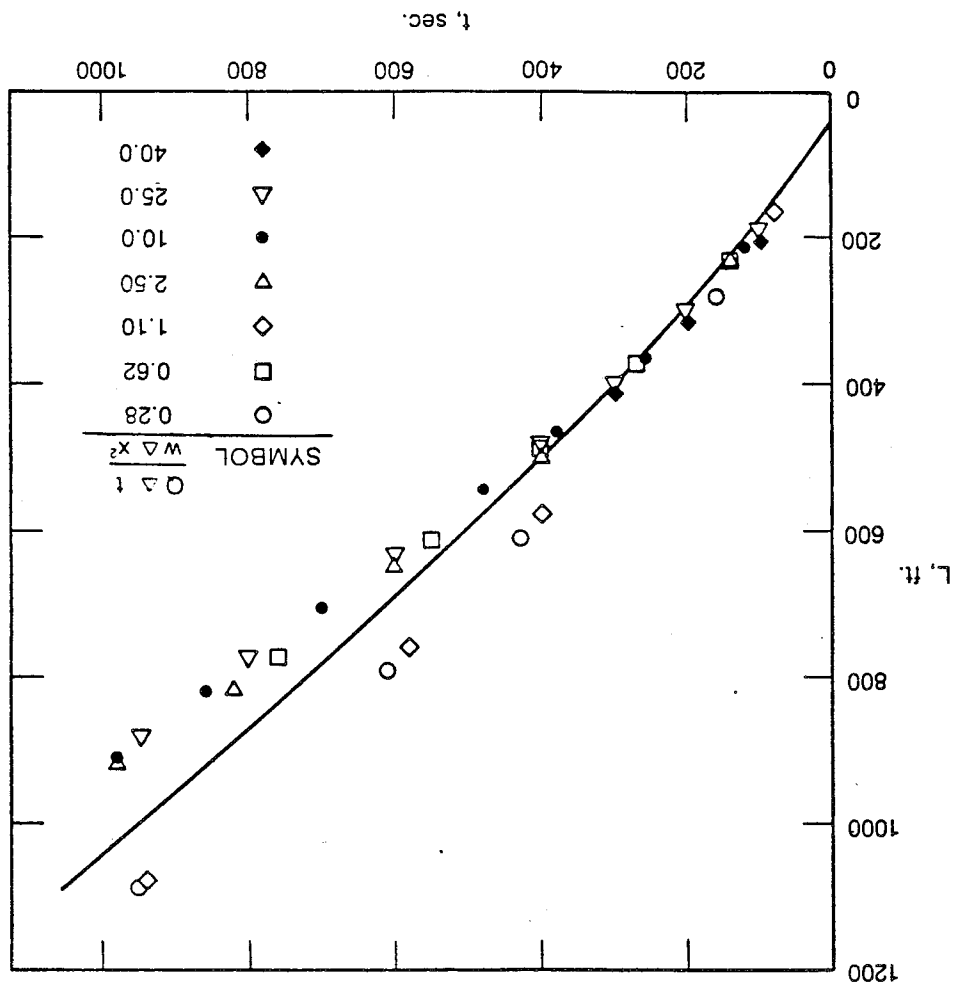
$$\xi = 1/4 + (\Delta t/\Delta x^2) \sin^2 \alpha \quad [39]$$

geometry of the system studied. Therefore, the term The constant, α , is a positive real number representing the

$$\xi = 1/4 + (\Delta t/\Delta x^2) \sin^2 \alpha \quad [38]$$

where,

Figure 13. Demonstration of Convergence of Current Model by Comparison with PKN Solution



To study the effects of timestep size in the dynamic growth model, a fracture model based on a ten foot mesh size was used. The model consisted of nine nodes vertically and ten horizontally, with a fracture occupying a space of three nodes vertically and four nodes horizontally. Three rows of nodes above and below the fracture were assigned higher confining stress to partially contain the vertical growth of the fracture. Effects of injection of 100 cp fluid at a rate of 1.0 ft³/sec. into the fracture were studied using timestep sizes of 0.1, 1.0, and 10.0 seconds. Injection was

Time Requirements of the Numerical Model:

There are some indications that the solution may be nearing the limit of stability at a value of D of approximately 40 or higher. Over the length of the test presented here, the fracture length and width for the case, D=40, conform well to the other solutions obtained. However, some uneven fracture growth at the leading edge is indicated.

slightly, but results in a stable solution. error introduced alters the fracture growth characteristics nodes and two flanking boundary layers. The discretization fracture to be defined by only one row of open fracture thirty-foot node size. The coarse grid size allows the rather than stability. These two cases were run using a 0.28 and 1.10, and the other results is related to node size

continued for 30 seconds to study the propagation of the initial fracture.

The model study conducted with 0.1 second timesteps required 300 timesteps to reach 30 seconds of injection. Output from the program was produced at eight times, representing fracture extension into various new nodes. This case required 56 seconds of cpu time to reach 30 seconds of pumping time. Time requirements for each timestep ranged from 0.1 to 0.3 seconds. Commonly, three iterations were required for each timestep.

The run conducted using 1.0 second timesteps required approximately 13 seconds of cpu time to reach 30 seconds of pumping time in 30 timesteps. Output was produced at seven timesteps. Time requirements were about 0.6 seconds per timestep with an average of six iterations per timestep.

The 10.0 second-timestep run required 5.7 seconds of cpu time to reach 30 seconds of pumping time in three timesteps. Output was generated at two timesteps during this run. Time requirements varied from approximately 1.4 to 2.9 seconds per timestep. Seven to twelve iterations were required for each timestep.

In summary, time requirements of approximately 0.1 to 0.2 seconds of cpu time per iteration for a small model are common. For comparison, execution times for the B7900 computer used here are similar to those of a VAX-11/780.

According to Hubbert (37) and Cleary (36) a hydraulic fracture will be initiated at some point in a wellbore where conditions of stress or rock strength are most advantageous. The effects on fracture geometry of the location of the point at which the fracture starts can be studied using a simple dynamic model. A fracture model grid is set up which is comprised of a target layer, in which the base case data are used, surrounded by confining layers with a principal confining stress 1000 psi greater than the target layers. A tensile strength of 1000 psi was also used in the confining layers to assure fracture containment:

Fracture Growth from Various Points of Initiation:

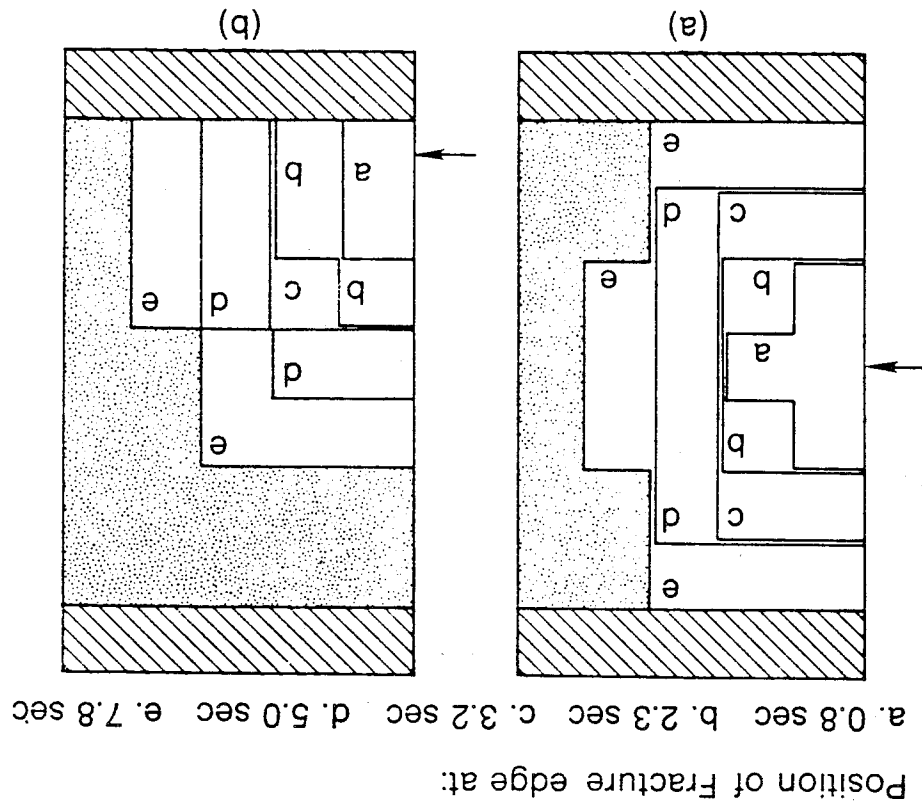
Many studies can be conducted using the dynamic fracture propagation model. These can lead insight into the effects of point of fracture initiation, confining stress variations, elastic property changes and fracturing fluid properties on hydraulic fracture geometry. Examples of simulation studies which can be run using the fracture propagation model to quantify the effects of these parameters are presented. Unless otherwise specified, the base case data defined by Eq. 35 with a tensile strength of 200 psi and a fluid viscosity of 100 cp, are used in all cases.

DYNAMIC FRACTURE PROPAGATION STUDIES

In one case, the fracture is presumed to initiate at the center of the target formation. Fracturing fluid enters the crack at this point and the fracture propagates radially outward until the effects of the confining layers are felt. The wellbore is modeled as an open-hole completion. This allows fluid to enter any open fracture node adjacent to the wellbore. Figure 14a shows the fracture propagation for the first 7.8 seconds of injection at a rate of 1.0 ft.³/sec. (10.7 bbl/min). The arrow indicates the point of fracture initiation. The created fracture is symmetrical about the point of initiation until the bounding layers (shown in cross-hatching) are reached. After approximately 8 seconds the fracture growth is confined in the vertical direction and the fracture propagates laterally through the target layer. Maximum created fracture width occurs at the center of the fracture, near the wellbore. This width was calculated to be 0.0092 ft. after 8 seconds. *

Figure 14b is a plot of the propagating fracture position for a crack initiated at the lower edge of the target formation, as indicated by the arrow. Fracture propagation is roughly symmetric about the point of fracture initiation, although no downward propagation occurs because of the presence of the confining layer. After approximately 8 seconds, the maximum fracture width is 0.010 ft. The frac-

Figure 14. Effect of Point of Initiation on Fracture Growth



One of the most important considerations in fracture design is containment of the fracture in the target formation. According to Teufel and Clark (42), among others, the principal factors controlling fracture confinement in layered rock systems are: 1) differences in mechanical properties, including elastic modulus and rock strength, 2) changes in confining stress in adjacent rock layers, and 3) shear strength of the interface. Their experimental work shows that shear strength of a material interface can contribute to fracture confinement. If an interface is weak enough to allow the adjacent rock layers to slip, the vertical fracture propagation can be stopped. Other research has shown that a sufficient normal stress across even an unbonded interface will generate a sufficient friction force to cause the interface to appear well bonded (40,42,43). The present

Hypothetical Studies of Fracture Containment:

For a vertically confined fracture. seems to be an important consideration only in early times widths. Based on these results, the point of initiation both cases yield roughly similar fracture geometries and only. After approximately fifteen seconds of propagation fracture proceeds to propagate in the horizontal direction the upper confining layer is reached. At this point the fracture continues propagating vertically and laterally until

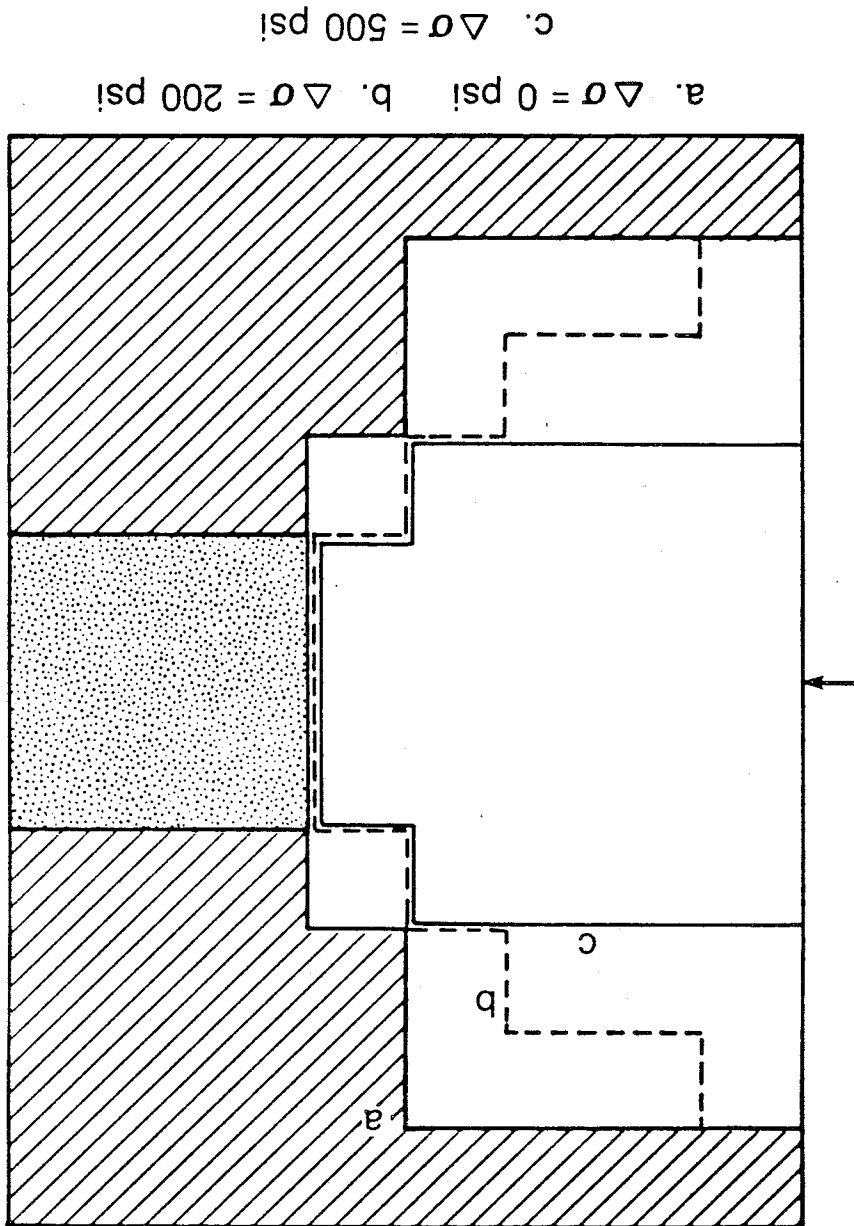
A fracture grid composed of a thirty-foot thick target layer bounded by forty-foot thick adjacent layers was used to demonstrate the ability of the current model to predict the effects of stress variation on fracture containment. Using the base case elastic properties and stresses, a fracture geometry was generated for a homogeneous system. After fifteen seconds of injection at a rate of $1.0 \text{ ft}^3/\text{sec}$, the fracture shape shown in Figure 15 as curve (a) was generated. An increase of 200 psi in the confining stress in the bounding layers causes a partial containment of the frac-

independently of other rock properties. merical model allows the effects of stress to be analyzed tectonic activity including thrusting and faulting. The nu- be transmitted differently in horizontal directions, and elastic properties of rocks which cause a vertical stress to Among the causes of stress variations are differences in layered rock systems can be generated by several mechanisms. effect on fracture geometry. Confining stress variations on stated that confining stress variations have a significant Teufel and Clark (42) and Warpinski, et al (44), demon-

Effects of Confining Stress

and mechanical properties can, however, be investigated. model is unable to study the effects of frictional or un- bonded interfaces. Effects of variation in confining stress

Figure 15. Effects of Difference in Confining Stress in Adjacent Layers on Fracture Containment



The result of this case, again after fifteen seconds of injection, is shown by curve (b) in Figure 15. Note that the fracture propagates deepest into the boundary layers at the near-wellbore edge of the fracture. This excess penetration results from high fluid pressures in the fracture. As fracture fluid pressure declines with length, less penetration into the bounding layers is developed.

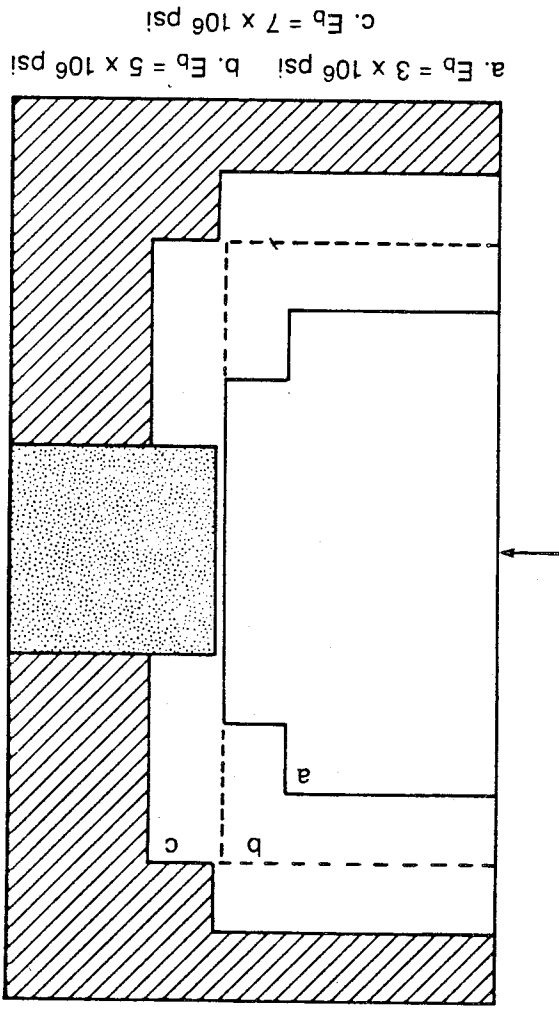
As discussed by Perkins and Kern (13), the high stresses in the boundary layers eventually establish an equilibrium fracture height. When this occurs, the walls of the fracture behave like levers in equilibrium, where the fracture fluid acts on one lever arm (from the fracture center to the edge of the confining bed) and the high confining stresses act on the shorter lever arm (the length of fracture penetration into the confining layer). When the confining stresses are increased to 500 psi above the stress in the target formation curve (c), the penetration into the boundary layers is further reduced. Under these stress conditions, an equilibrium fracture height of approximately fifty feet is developed and maintained throughout the length of the fracture propagation process studied. These results agree with physical observations made in Sandia Laboratories mineback experiments (44). In these studies a difference in confining stress of 300 psi was found sufficient to contain fractures.

The effects of elastic property variations on fracture containment have only recently been identified through experimental research (44,46). Both in large scale fracture mineback studies and in laboratory scale experiments it has been shown conclusively that high elastic moduli in bounding layers cannot alone cause the containment of a hydraulic fracture. As previously discussed, however, the effects of elastic properties on stresses can, and often do, control fracture containment. Many recently proposed models, such as that of Simonson and Abou-Sayed (47), which rely on

Effects of Elastic Properties

Another analogous effect, which can be important in fracturing porous media, is discussed by Cleary (45). Because the definition of effective stress includes both confining stress and formation pore pressure, an identical effect can be generated by reducing the formation pore pressure of the target layer. This has the effect of transmitting a higher effective stress to the fracture walls over the interval influenced by the pressure reduction. In the absence of fluid leakoff, the current model predicts identical results for the same variation in pore pressure or confining stress. If this prediction can be supported experimentally, it could offer a useful tool for engineering fracture containment.

Figure 16. Effects of Elastic Property Variation on Fracture Containment



reports that in fracture mineback experiments a variation in elastic modulus of a factor of fifteen did not cause fracture containment. In fact, in six out of six tests in which fractures were initiated near a material interface, the fractures tended to preferentially propagate into the higher modulus material rather than in the low modulus material in which they were initiated.

The enhanced propagation in material of high elastic modulus appears to be related to the high stresses required to cause a displacement in such a medium. A large pressurized "lever arm" of the fracture face in a low modulus medium generates a tendency to displace the adjacent layers in the high modulus material. To overcome this tendency a large tensile stress is developed in the high modulus material because of its rigidity. In the current formulation of the model, these tensile stresses rapidly approach the tensile strength of the material and rupture occurs.

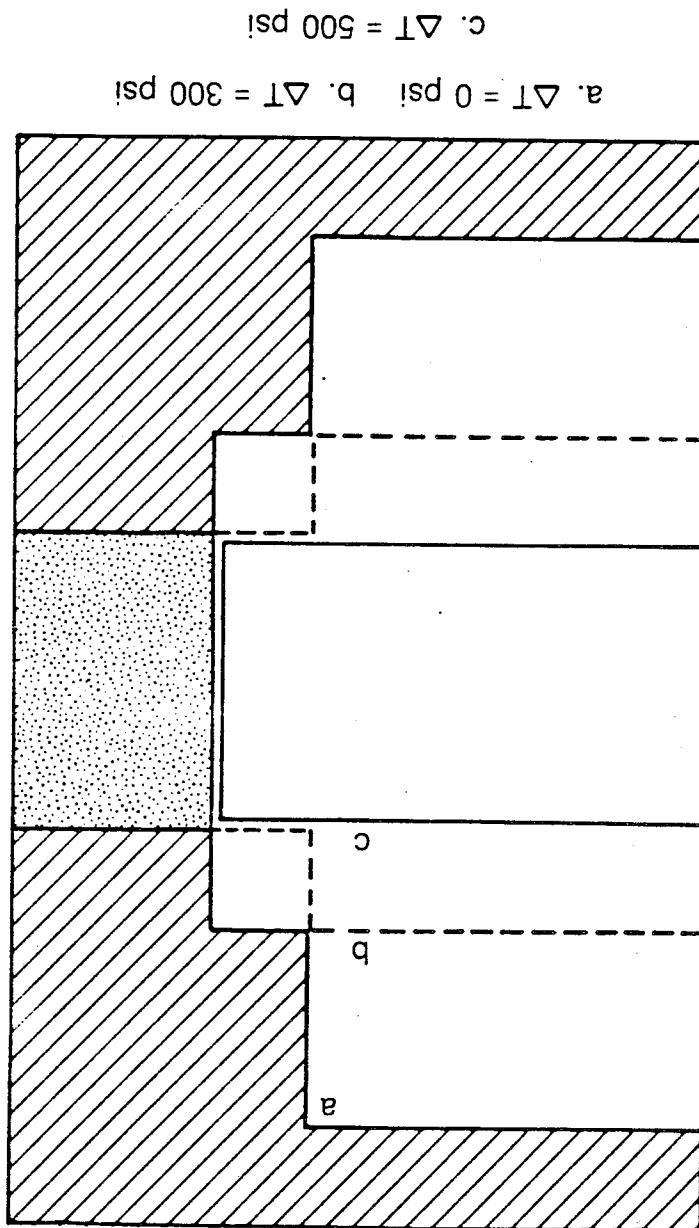
Effects of Tensile Strength

An analysis of the predicted effect of material tensile strength was conducted using a similar fracture geometry. All rock properties and stresses were set at the base case values and only tensile strength of the boundary layers was varied. The base case tensile strength in the target layer was 200 psi. This value was used in the boundary layers to

generate a roughly symmetrical fracture geometry as shown in Figure 17, curve a. The coarse mesh size used in this study causes the blockish fracture shape. An increase in the tensile strength of the boundary layers to 500 psi causes significant confinement of the fracture as indicated by the position of the fracture boundary in Figure 17 (curve b) after fifteen seconds of injection. An increase in tensile strength to only 700 psi (curve c) causes complete containment of the fracture in the target zone. These magnitudes of rock tensile strength are not unrealistic for actual systems. Warpinski (44) has reported measured tensile strengths of Tennessee sandstone of up to 1700 psi. Tensile strengths of up to 3000 psi are not uncommon in some limestone (48).

A secondary effect of high tensile strength is the increase in fracture width corresponding to a well contained geometry. The maximum fracture width obtained in the unfined case (curve a), after fifteen seconds, was 0.0096 ft. For the well confined case, (curve c), the fracture width increased to 0.0123 ft. in the same time. The increase in width results from the higher net stress applied to the walls of the pressurized fracture. A 700 psi tensile strength supports a net stress at the center of the fracture of approximately 640 psi, while the 200 psi strength can

Figure 17. Effect of Tensile Strength Variation on Fracture Containment in a Layered System



support only 330 psi of net stress for the same grid geometry.

These hypothetical test cases indicate the relative importance of various parameters to fracture containment. In general, the principal controlling factors appear to be material tensile strength and net stress applied to the fracture walls. This finding suggests that some control over fracture containment can be exercised when non-penetrating fracturing fluids are used. Pressure drawdown of the target formation may influence fracture containment around the wellbore, as suggested by Cleary (45). Matrix acidizing, to decrease the tensile strength of the target zone may also provide some beneficial effects.

While hypothetical cases give some insight into potential fracture containment strategies, an experimental verification of model predictions is always necessary. In connection with their fracture mineback studies, Sandia National Laboratories has conducted a series of small scale experimental fracturing studies which have been well documented by Warpinski, et al (44). Several of these studies were used as test cases for comparison with model predictions.

In one series of experiments cylindrical samples of Ash-Fall Tuff, eight inches in diameter and eight inches long, were subjected to various confining stresses. A hydraulic fracture was initiated in the upper half of the sample. In one case, a 300 psi confining stress was applied to the upper half of the sample during fracturing. A test was then conducted on a separate sample with stress applied to the lower half. Stress levels in the tuff samples were computed using a finite element technique. Results of the experiment showed that the applied stresses were sufficient to control the direction of fracture propagation.

These experiments were modeled using a 25X10 grid composed of squares 0.0417 ft. on a side. The stress levels

COMPARISON OF DYNAMIC GROWTH MODEL WITH EXPERIMENTAL RESULTS

A similar set of experiments was conducted on samples composed of two blocks of Tennessee Sandstone (44). Confining stresses were applied to either the upper or lower sample sections, then the two sections were pressed together by a vertical, normal stress of 3000 psi. This vertical stress insured sufficient friction at the sample interface to prevent slippage. By this means a discontinuous stress field

very good. Agreement in both the top and bottom stressed experiments is experimentally observed fracture shape (dashed lines). ries from the current model (solid lines) compared with the presentation of the numerically predicted fracture geometries as a block modeling the existing cavity. Figure 19 is a re-jection is shown by an arrow in Figure 18 and in Figure 19 cavity in the sample were conducted. The point of fluid injection is shown by an arrow in Figure 18 and in Figure 19 viscosity liquid at a rate of $1.6 \text{ cm}^3/\text{sec}$ into an existing Numerical simulation of injection of a one centipoise

$$\begin{aligned}
 E &= 1.2 \times 10^6 \text{ psi} \\
 \nu &= 0.15 \\
 T &= 450 \text{ psi} \\
 k &= 0.01 \text{ md.}
 \end{aligned}$$

reported for the Ash-Fall Tuff are: Figures 18a and 18b, respectively. Mechanical properties bottom-stressed and top-stressed experiments as shown in reported by Warpinski, et al, were input to the grid for the

Figure 18. Representation of Stress Distribution in Ash-Fall Tuff Samples with a) Stress Applied to Lower Half, and b) Stress Applied to Upper Half

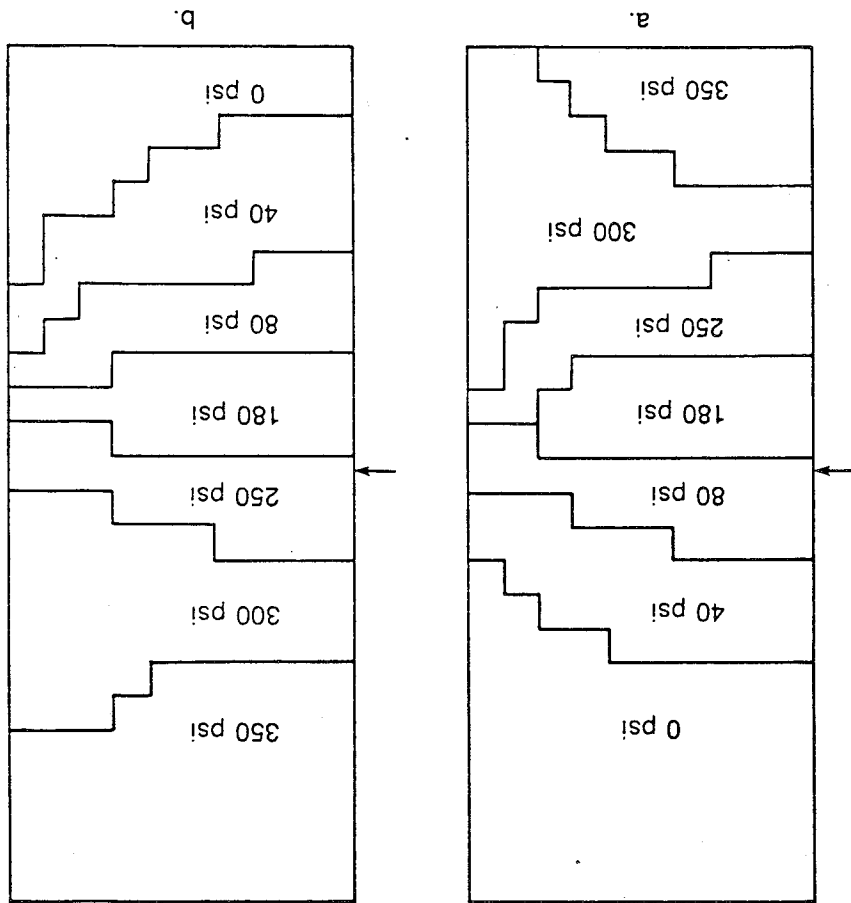
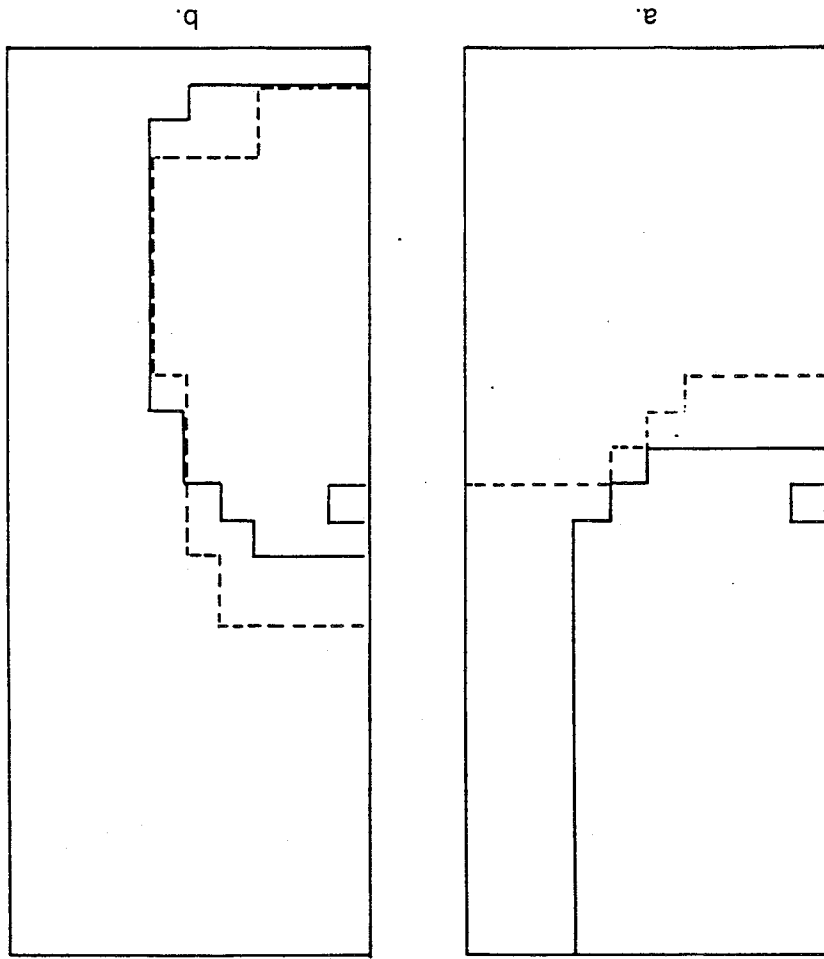


Figure 19. Comparison of Predicted and Experimental Fracture Propagation in a) Bottom-Stressed and b) Top-Stressed Ash-Fall Tuff Samples



Model Prediction ———
Experimental Result - - - -

could be approximated in the samples. Properties of

Tennessee Sandstone are reported as:

$$E = 7.18 \times 10^6 \text{ psi}$$

$$\nu = 0.08$$

$$T = 1740 \text{ psi}$$

$$k = 0.01 \text{ md}$$

Three experiments were modeled using the dynamic propa-

gation simulator. In the first case no confining stress was

applied to either section of the sample. The result, Figure

20a, is an approximately radially symmetric crack. The

fracture extends across the boundary between the two sample

sections, shown as the dashed line, without a noticeable ef-

fect on fracture shape. The experimental results (in dotted

line) show the same type of fracture propagation. In the

laboratory samples, the effects of the sample boundary cause

the fracture to propagate more quickly toward one edge of

the block (44). Excluding this the fracture is roughly cir-

cular and symmetric about the point of initiation.

The second simulated case modeled a fracture initiated

in the upper sample section with a 250 psi confining stress

applied to the lower section. The results, Figure 20, show

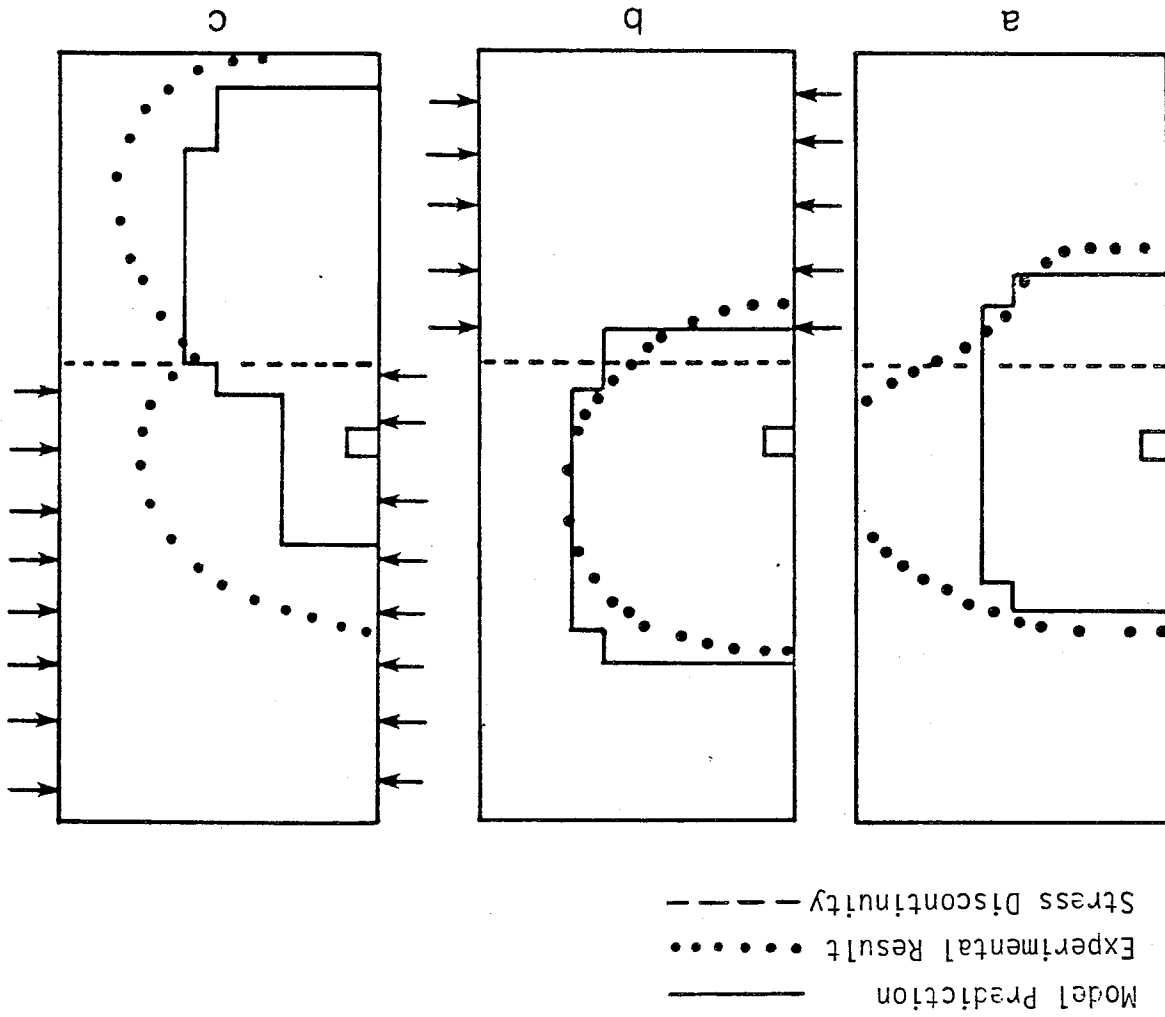
that the downward fracture propagation is halted after a

slight penetration into the high stress layer. Experiment-

tally reported results are almost identical to the predicted

fracture shape.

Figure 20. Simulation Results of Fracture Propagation in Layered Tennessee Sandstone Samples Under a) No Confining Stress, b) 250 psi Stress on Lower Section, and c) 1000 psi Stress on Upper Section.



One of the few parameters subject to external control which can affect hydraulic fracture geometry is the hydrau-

Viscosity Effects

Effects of Fracturing Fluid Properties:

Comparison of predictions of this model with experimental results for these small scale laboratory samples shows good agreement in fairly complex geometries. The predicted effects of variation in stress and elastic properties are similar to those noted in laboratory studies. These results indicate that the model is capable of predicting fracture geometries under well defined stress conditions.

The third case studied (Figure 20) involves the effect of a 1000 psi confining stress on the upper sample section, propagated outward from the point of initiation faster than it grew downward. This resulted in a large diameter radial fracture in the high stress layer. In the experimental case, the fracture propagated outward from the point of initiation faster than it grew downward. This resulted in a large diameter radial fracture in the high stress layer. The principal difference between the predicted and experimental results is the radius of the fracture in the lower stress region. Experimental results show a similar trend. The principal difference between the predicted and experimental results is the radius of the fracture in the high-stress layer. In the experimental case, the fracture propagated outward from the point of initiation faster than it grew downward. This resulted in a large diameter radial fracture in the high stress layer.

Simulation of the injection of Newtonian fluids of 100, 500, and 1000 cp at a rate of 1 ft³/sec. (10.7 bbl/min.) in- to one fracture wing, showed that a radially symmetric frac- ture will be generated. Varying the fluid viscosity over the stated range had no effect on fracture extension after up to fifteen seconds of injection. However, the fracture width distribution was significantly changed. The 100 cp fluid injection case yielded a maximum fracture width, after fifteen seconds, of 0.0096 ft. Increasing viscosity to 500 cp increased the width at the wellbore to 0.0132 ft. while the 1000 cp fluid generated a width of 0.0151 ft. In the same time. High fracture fluid viscosity also tended to create a wider distribution of fracture widths, generating a much thinner fracture near the leading edge.

Other cases studied using the current model involving the propagation of a partially contained fracture indicate

the fracturing fluid. Fracturing fluid viscosity can be changed in an effort to optimize fracture design. A series of simulation studies was conducted holding all rock proper- ties constant. A uniform elastic medium, with no rock lay- ers, as defined by the previously used base case data, was used for part of the study. A Newtonian fluid viscosity was used to eliminate the effects of shear rate from the re- sults.